DAM-BREACH FLOODS

D. L. Fread
Director, Hydrologic Research Laboratory
NOAA, National Weather Service
Office of Hydrology
1325 East-West Highway, RM 8348
Silver Spring, Maryland 20910
USA

5.1 INTRODUCTION

Dams provide society with essential benefits such as water supply, flood control, recreation, hydropower, and irrigation. However, catastrophic flooding occurs when a dam fails and the impounded water escapes through the breach to cause death and destruction of people and their developments existing in the downstream valley. Usually, the magnitude of the flow greatly exceeds all previous floods and the response time available for warning the populace is much shorter than for precipitation-runoff floods. According to reports by the International Commission on Large Dams (ICOLD, 1973) and the United States Committee on Large Dams in cooperation with the American Society of Civil Engineers (ASCE/USCOLD, 1975), about 38 percent of all dam failures are caused by overtopping of the dam due to inadequate spillway capacity and by spillways being washed out during large inflows to the reservoir from heavy precipitation runoff. About 33 percent of dam failures are caused by seepage or piping through the dam or along internal conduits, while about 23 percent of the failures are associated with foundation problems, and the remaining failures are due to slope embankment slides, damage or liquefaction of earthen dams from earthquakes, and overtopping of the dam by landslide-generated waves within the reservoir. Middlebrooks (1952) describes earthen dam failures that occurred within the United States prior to 1951. Johnson and Illes (1976) summarize 300 dam failures throughout the world.

The potential for catastrophic flooding due to a dam failure (breach) was brought to the attention of politicians, emergency action personnel, engineers, and portions of the general populace within the United States during the 1970's by several catastrophic floods due to dam failures, i.e., the Buffalo Creek coal-waste dam in 1972, the Teton Dam in 1976, the Laurel Run Dam in 1977, and the Kelly Barnes Dam in 1977.

The Buffalo Creek coal-waste dam collapsed (Davies et al., 1975) on the Middle Fork, a tributary of Buffalo Creek in southwestern West Virginia near Saunders. Most of the dam was eroded away very rapidly on February 26, 1972, due to overtopping waters; the breached dam released about 500 acre-ft of impounded waters into Buffalo Creek valley, causing the most catastrophic flood in the state's history with the loss of 118 lives, 500 homes, and property damage exceeding $50 million.

The Teton Dam near Sugar City, Idaho, a 300 ft high earthen dam with 250,000 acre-ft of stored water, failed (Ray et al., 1976) on June 5, 1976, due to internal piping, killing 11

people, making 25,000 homeless, and inflicting about $400 million in damages to the downstream Teton-Snake River Valley.

The 45-ft high earthen embankment Laurel Run Dam near Johnstown, Pennsylvania, was overtopped and breached (Chen and Armbruster, 1980) July 20, 1977, releasing 450 acre-ft of stored water. This resulted in the death of 40 people and heavy property damages.

The Kelly Barnes Dam near Toccoa, Georgia, an earthen embankment dam reconstructed several times, finally reaching a height of about 35 ft, with 600 acre-ft of storage, was overtopped and subsequently breached (Federal Investigative Board, 1977) November 6, 1977. This resulted in the death of 39 people who resided about 0.75 mile downstream of the dam.

Within the United States, as well as in many nations throughout the world, there are many dams that are 30 or more years old, and many of the older dams are a matter of serious concern because of increased hazard potential due to downstream development and increased risk of failure due to structural deterioration and/or inadequate spillway capacity. A report by the U.S. Army (1981) gives an inventory of the approximately 70,000 dams within the United States with heights greater than 25 ft or storage volumes in excess of 50 acre-ft. The report also classifies some 20,000 of these as being "so located that failure of the dam could result in loss of human life and appreciable property damage ..."

In addition to the man-made dams described above, natural formed dams can also produce dam-breach floods. Occasionally dams are formed naturally when a landslide blocks a river that traverses through rugged terrain. Eventually the landslide-formed dam is overtopped by the blocked and ponded river flow, and a breach is eroded through the naturally formed dam creating a dam-breach flood.

A distinguishing feature of dam-breach or dam-break floods is the great magnitude of the peak discharge when compared to any precipitation runoff-generated floods that could occur in the same valley. The dam-break flood is usually many times greater (an order of magnitude or more) than the runoff flood of record. Another distinguishing characteristic of dam-break floods is the extremely short time from beginning of rise until the occurrence of the peak and very short total duration time of the flood. The time to peak, in almost all instances, is synonymous with the interval of time required for the breach (failure) to develop completely once it starts to form. This time of failure is of the order of minutes for most dams, although some very large dams may have a time of failure of an hour or greater. This characteristic, along with the great magnitude of the peak discharge, causes the dam-breach flood wave to have acceleration components of a far greater significance that those associated with a precipitation runoff-generated flood and helps to produce significant wave peak attenuation.

5.2 BREACH DESCRIPTION

The breach is the opening formed in the dam as it fails. The actual failure mechanics are understood only partially for earthen dams and less for concrete dams. Prior to about 1970, efforts to predict downstream flooding due to dam failures usually assumed that the dam failed completely and instantaneously, e.g., Ritter (1892), Schocklitsch (1917), Ré (1946), Dressler (1954), Stoker (1957), Su and Barnes (1969), and Sakkas and Strelkoff (1973). Others, such as the Army Corps of Engineers (1960) recognized the need to assume a partial rather than complete breach; however, it was still assumed the breach occurred instantaneously. The assumptions of instantaneous and complete breaches were used for reasons of convenience when applying certain mathematical techniques for analyzing dam-breach flood waves. The assumptions are somewhat appropriate for concrete arch dams, but

are not appropriate for earthen dams and concrete gravity dams. For these dams, as well as well concrete arch dams, the breach should be considered (1) to develop over a finite interval of time (τ) and (2) to encompass only a portion of the dam except for concrete arch dams (Fread and Harbaugh, 1973; Fread, 1977).

Partial dam breaches with $\tau > 0$ result in considerably smaller dam-breach floods than instantaneous ($\tau = 0$) and complete breaches. It is readily apparent that a smaller breach will allow less peak outflow than a larger breach; however, it is not quite as apparent that a larger failure time results in less peak outflow. As the dam breach forms, the outflow through the breach reduces the reservoir storage contained by the dam, resulting in a reduction of the reservoir water level. The rate of flow through the breach is proportional to the height (head) of the water above the breach bottom (as in weir-type flow). Therefore, as the breach forms, the water level reduces; and when the breach is fully formed, the resulting head of water is less than that if the breach formed instantaneously or even at a faster rate. The smaller head of water available to produce flow through the breach when it completely forms (both in the vertical and horizontal directions) results in a smaller peak outflow and a smaller dam-breach flood. The extent of flood peak reduction due to a larger failure time is directly proportional to the magnitude of the final breach width and inversely proportional to the magnitude of the reservoir storage volume.

5.2.1 Mathematical Description of Breach

The breach may be described mathematically using the following parameters: the time of failure (τ), the terminal bottom width parameter (b), another parameter (z) which provides for breach shapes of rectangular, triangular, or trapezoidal. The parametric approach is convenient in predicting dam-breach floods for reasons of simplicity, generality, wide applicability, and the uncertainty in the actual failure mechanism. The parametric approach to the breach description follows that used by Fread and Harbaugh (1973) and later by Fread (1977, 1985, 1988).

The shape parameter (z) is the side slope of the breach, i.e., 1 vertical:z horizontal. The value for z varies from 0 to about unity. Its value depends on the angle of repose of the compacted and wetted materials composing the dam and through which the breach develops. Rectangular, triangular, or trapezoidal shapes may be specified by using various combinations of values for z and b, e.g., $z=0$ and $b>0$ produces a rectangular-shaped breach, and $z>0$ and $b=0$ yields a triangular-shaped breach. The terminal bottom width (b) is related to the average width of the breach ($\bar{b}$) by the following:

$$b = \bar{b} - zH_d \tag{5.1}$$

in which H_d is the height of the dam. In the parametric description of the breach, the breach bottom width starts at a point at the crest of the dam (see Fig. 5.1) and enlarges at a linear or nonlinear rate over the failure time (τ) until the terminal bottom width (b) is attained and the breach bottom has eroded to the minimum elevation, h_{bm}. The instantaneous bottom elevation of the breach is described as a function of time (t_b) according to the following:

$$h_b = h_d - (h_d - h_{bm})(t_b/\tau)^\rho \qquad 0 \le t_b \le \tau \tag{5.2}$$

in which h_d is the elevation of the top of the dam, h_{bm} is the final elevation of the breach bottom which is usually, but not necessarily, the bottom of the reservoir or outlet channel bottom, t_b is the time since beginning of breach formation, and ρ is the parameter specifying

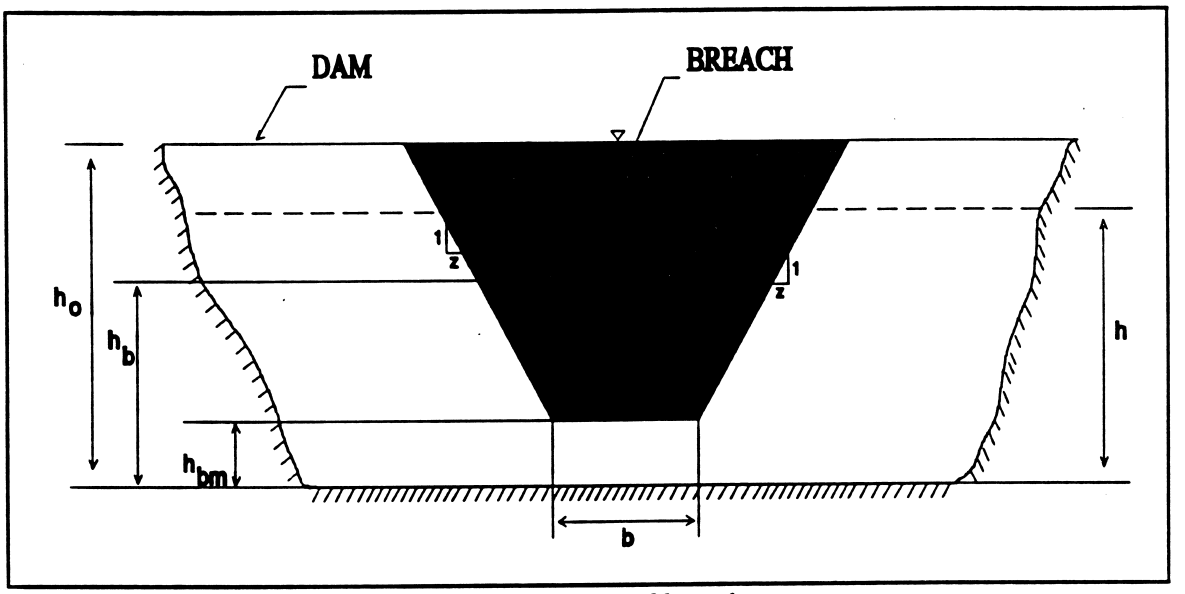

Figure 5.1 Front view of dam showing formation of breach

the degree of nonlinearity, e.g., $\rho=1$ is a linear formation rate, while $\rho=2$ is a nonlinear quadratic rate; the range for ρ is $1 \leq \rho \leq 4$, with the linear rate usually assumed. The instantaneous bottom width (b_i) of the breach is given by the following:

$$b_i = b(t_b/\tau)^\rho \qquad 0 \leq t_b \leq \tau \tag{5.3}$$

When simulating a dam failure, the actual breach formation can commence when the reservoir water surface elevation (h) exceeds a specified value, h_f. This feature permits the simulation of an overtopping of a dam in which the breach does not form until a sufficient amount of water has passed over the crest of the dam to have eroded away the downstream face of the dam. The breach can also commence when a specified start-of-failure (t_f) time is reached in the simulation. A piping failure may also be simulated by specifying the initial centerline elevation of the pipe, using Eqs. (5.2)-(5.3), letting the top of the pipe form at the same rate as the bottom of the pipe, and letting $z = 0$. It is possible to also limit the breach formation to only the spillway section of the dam.

5.2.2 Concrete Dams

Concrete gravity dams tend to have a partial breach as one or more monolith sections formed during the construction of the dam are forced apart and over-turned by the escaping water. The time (τ) for breach formation is in the range of a few minutes depending on the number of monoliths that fail in succession. It is difficult to predict the number of monoliths which may be displaced or fail; however, by using a dam-breach flood prediction model such as described later in Section 5.3.1.5, and making several separate applications of the model wherein the breach width parameter (b) representing the combined lengths of assumed failed monoliths is varied in each application, the resulting reservoir water surface elevations can be used to indicate the extent of reduction of the loading pressures on the dam. Since the loading diminishes as b is increased, a limiting safe loading condition which would not cause further failure may be estimated. Unlike the concrete gravity dams, concrete arch dams tend to fail completely and are assumed to require only a few minutes for the breach formation.

The shape of the breach is usually approximated as rectangular for either gravity or arch concrete dams; this is accomplished by using a value of zero for the shape parameter (z).

5.2.3 Earthen Dams

Earthen dams which exceedingly outnumber all other types of dams do not tend to completely fail, nor do they fail instantaneously. The fully formed breach in earthen dams tends to have an average width ($\bar{b}$) in the range ($H_d \leq \bar{b} \leq 5H_d$) where H_d is the height of the dam. The middle portion of this range for $\bar{b}$ is supported by the summary report of Johnson and Illes (1976) and the upper range by the report of Singh and Snorrason (1982). Breach widths for earthen dams are therefore usually much less than the total length of the dam as measured across the valley. Also, the breach requires a finite interval of time (τ) for its formation through erosion of the dam materials by the escaping water. Total time of failure (for overtopping) may be in the range of a few minutes to usually less than an hour, depending on the height of the dam, the type of materials used in construction, the extent of compaction of the materials, and the magnitude and duration of the overtopping flow of the escaping water. The time of failure (τ) as used herein is the duration of time between the first breaching of the upstream face of the dam until the breach is fully formed. For overtopping failures, the beginning of breach formation at the upstream face of the dam occurs after the downstream face of the dam has eroded away and the resulting crevasse has progressed back across the width of the dam crest to reach the upstream face.

Piping failures occur when initial breach formation takes place at some point below the top of the dam due to erosion of an internal channel through the dam by the escaping water. Times of failure are usually considerably longer for piping than overtopping failures. As the erosion proceeds, a larger and larger opening is formed; this is eventually hastened by caving-in of the top portion of the dam.

Poorly constructed coal-waste (mine tailings) dams which impound water tend to fail more rapidly than well-designed dams and have average breach widths in the upper range of those for the earthen dams.

5.2.3.1 Statistically-Based Breach Predictors. Some statistically derived predictors for $\bar{b}$ and τ have been presented in the literature, i.e., MacDonald and Langridge-Monopolis (1984) and Froehlich (1987, 1995). Using Froehlich's data of the properties of 63 breaches of dams ranging in height from 12 to 285 ft, with 6 of the dams greater than 100 ft, the following predictive equations were obtained:

$$\bar{b} = 9.5\, k_o\, (V_r H_d)^{0.25} \tag{5.4}$$

$$\tau = 0.59\, V_r^{0.47} / H_d^{0.91} \tag{5.5}$$

in which $\bar{b}$ is average breach width (ft), τ is time of failure (hrs), $k_o = 0.7$ for piping and 1.0 for overtopping, V_r is volume (acre-ft) and H_d is the height (ft) of water over the breach bottom (H_d is usually about the height of the dam). Standard error of estimate for $\bar{b}$ was ± 82 ft which is an average error of ± 56 percent of $\bar{b}$, and the standard error of estimate for τ was ± 1.1 hrs which is an average error of ± 86 percent of τ.

5.2.3.2 Physically-Based Breach Erosion Models. Another means of determining the breach properties is the use of physically-based breach erosion models. Cristofano (1965) modeled the partial, time-dependent breach formation in earthen dams; however, this procedure

required critical assumptions and specification of unknown critical parameter values. Also, Harris and Wagner (1967) used a sediment transport relation to determine the time for breach formation, but this procedure required specification of breach size and shape in addition to two critical parameters for the sediment transport relation. Then, Ponce and Tsivoglou (1981) presented a rather computationally complex breach erosion model which coupled the Meyer-Peter and Muller sediment transport equation to the one-dimensional differential equations of unsteady flow (Saint-Venant equations) and sediment conservation. They compared the model's predictions with observations of a breached landslide-formed dam on the Mantaro River in Peru. The results were substantially affected by the judicious selection of the breach channel hydraulic friction factor (Manning n), an empirical breach width-flow relation parameter, and an empirical coefficient in the sediment transport equation.

Another physically-based breach erosion model (BREACH) for earthen dams was developed (Fread, 1984, 1987) which substantially differed from the previously mentioned models. It predicted the breach characteristics (size, shape, time of formation) and the discharge hydrograph emanating from a breached earthen dam which was man-made or naturally formed by a landslide. The model was developed by coupling the conservation of mass of the reservoir inflow, spillway outflow, and breach outflow with the sediment transport capacity of the unsteady uniform flow along an erosion-formed breach channel. The bottom slope of the breach channel was assumed to be the downstream face of the dam. The growth of the breach channel was dependent on the dam's material properties (D_{50} size, unit weight, internal friction angle, cohesive strength). The model considered the possible existence of the following complexities: (1) core material properties which differ from those of the outer portions of the dam; (2) formation of an eroded ditch along the downstream face of the dam prior to the actual breach formation by the overtopping water; (3) the downstream face of the dam could have a grass cover or be composed of a material such as rip-rap or cobble stones of larger grain size than the major portion of the dam; (4) enlargement of the breach through the mechanism of one or more sudden structural collapses of the breaching portion of the dam due to the hydrostatic pressure force exceeding the resisting shear and cohesive forces; (5) enlargement of the breach width by collapse of the breach sides according to slope stability theory; and (6) the capability for initiation of the breach via piping with subsequent progression to a free-surface breach flow. The outflow hydrograph was obtained through a computationally efficient time-stepping iterative solution. This breach erosion model was <u>not</u> subject to numerical stability/convergence difficulties experienced by the more complex model of Ponce and Tsivoglou. The model's predictions were favorably compared with observations of a piping failure of the large man-made Teton Dam in Idaho, the piping failure of the small man-made Lawn Lake Dam in Colorado, and an overtopping activated breach of a large landslide-formed dam in Peru. Model sensitivity to numerical parameters was minimal; however, it was somewhat sensitive to the internal friction angle of the dam's material and the extent of grass cover when simulating man-made dams; and it was sensitive to the cohesive strength of the material composing landslide-formed dams. A reasonable variation of cohesion and internal friction angle parameters produced less than ± 20 percent variation in the breach properties.

Other physically-based breach erosion models include the following: (1) the BEED model (Singh and Quiroga, 1988) which is similar to the BREACH model except it considers the effect of saturated soil in the collapse of the breach sides and it routes the breach outflow hydrograph through the downstream valley using a simple diffusion routing technique (Muskingum-Cunge) which neglects backwater effects and can produce significant errors in routing a dam-breach hydrograph when the channel/valley slope is less than 0.003; (2) a numerical model (Macchione and Sirangelo, 1988) based on the coupling of the one-dimensional unsteady flow (Saint-Venant) equations with the continuity equation for sediment

transport and the Meyer-Peter and Muller sediment transport equation; (3) a numerical model (Bechteler and Broich, 1993) based on the coupling of the two-dimensional unsteady flow equations with the sediment continuity equation and the Meyer-Peter and Muller sediment transport equation; and (4) a series of analytical models (Singh and Quiroga, 1988) requiring calibration of critical parameters. A more detailed description of the BREACH model (chosen as a practical representative of physically-based breach models) follows.

5.2.3.3 BREACH Model. The BREACH model utilizes the principles of soil mechanics, hydraulics, and sediment transport to simulate the erosion and bank collapse processes which form the breach. Reservoir inflow, storage, and spillway characteristics, along with the geometrical and material properties of the dam (D_{50} size, cohesion, internal friction angle, porosity, and unit weight) are utilized to predict the outflow hydrograph. The essential model components are described as follows.

Reservoir level computation. Conservation of mass is used to compute the reservoir water surface elevation (h) due to the influence of a specified reservoir inflow hydrograph (Q_i), spillway overflow (Q_{sp}) as determined from a spillway rating table, broad-crested weir flow (Q_o) over the crest of the dam, broad-crested weir flow (Q_b) through the breach, and the reservoir storage characteristics described by a surface area (S_a)-elevation table. Letting Δh represent the change in reservoir level during a small time interval (Δt), the conservation of mass requires the following relationship:

$$\Delta h = \frac{0.0826\ \Delta t}{S_a} (\bar{Q}_i - \bar{Q}_b - \bar{Q}_{sp} - \bar{Q}_o) \tag{5.6}$$

in which the units of Δh, Δt, Q and S_a are ft, sec, ft^3/sec, and acre-ft, respectively, and the bar ($^-$) denotes the average value during the Δt time interval. Thus, the reservoir elevation (h) at time (t) can easily be obtained since $h = h' + \Delta h$, in which h' is the reservoir elevation at time $(t - \Delta t)$. If the breach is formed by overtopping, the breach outflow is simulated using a broad-crested weir flow equation, i.e.,

$$Q_b = 3\ A_b(h - h_b)^{0.5} \tag{5.7}$$

If the breach is formed by piping, a short-tube orifice flow equation is used to simulate the breach outflow, i.e.,

$$Q_b = A_b[2g(h - h_p)/(1 + fL/d_m]^{0.5} \tag{5.8}$$

in which A_b is the area (ft^2) of flow over the weir or orifice area, h_b is the elevation of the bottom of the breach at the upstream face of the dam, h_p is the specified center-line elevation of the pipe, f is the Darcy friction factor which is dependent on the D_{50} grain size, L is the length of the pipe, and d_m is the diameter or width of the pipe.

Breach width. Initially the breach is considered rectangular with the width (B_o) based on the assumption of optimal channel hydraulic efficiency, $B_o = B_r y_c$, in which y_c is the critical depth of flow at the entrance to the breach; i.e., $y_c = 2/3\ (h - h_b)$. The factor B_r is 2 for overtopping and 1 for piping. The initial rectangular-shaped breach can change to a trapezoidal shape when the sides of the breach collapse due to the breach depth exceeding the limits of a freestanding cut in soil of specified properties of cohesion (C), internal friction

angle (ϕ), unit weight (γ), and existing angle (θ') that the breach cut makes with the horizontal. The collapse occurs when the effective breach depth (d") exceeds the critical depth (d_c), i.e.,

$$d_c = 4C \cos \phi \sin \theta' / [\gamma - \gamma \cos(\theta' - \phi)] \tag{5.9}$$

The effective breach depth (d") is determined by reducing the actual breach depth (d) by $y_c/3$ to account for the supporting influence of the water flowing through the breach. The θ' angle reduces to a new angle (θ'') upon collapse which is simply $\theta'' = (\theta' + \phi)/2$.

Breach erosion. Erosion is assumed to occur equally along the bottom and sides of the breach except when the sides of the breach collapse. Then, the breach bottom is assumed not to continue to erode downward until the volume of collapsed material along the length of the breach is removed at the rate of sediment transport occurring along the breach at the instant before collapse. After this characteristically short pause, the breach bottom and sides continue to erode. Material above the wetted portion of the eroding breach sides is assumed to simultaneously collapse as the sides erode. Once the breach has eroded to the specified bottom of the dam, erosion continues to occur only along the sides of the breach. The rate at which the breach is eroded depends on the capacity of the flowing water to transport the eroded material. The Meyer-Peter and Muller sediment transport relation, as modified by Smart (1984) for steep channels, is used, i.e.,

$$Q_s = 3.64(D_{90}/D_{30})^{0.2} \frac{D^{2/3}}{n} P S^{1.1} (DS - 0.0054 D_{50} \tau_c) \tag{5.10}$$

in which Q_s is the sediment transport rate, D_{90}, D_{30}, and D_{50}, are the grain sizes in (mm) at which 90 percent, 30 percent, and 50 percent respectively of the total weight is finer, D is the hydraulic depth of flow computed from Manning's equation for flow along the breach channel at any instant of time, S is the breach bottom slope which is assumed to always be parallel to the downstream face of the dam, τ_c is Shield's critical sheer stress that must be exceeded before erosion occurs, and n is the Manning friction (roughness) coefficient which can be computed from the Strickler equation (Chow, 1959) for sand-bed channels or for gravel-bed channels (Jarrett, 1984) or simply estimated. The Δd incremental thickness eroded from the breach bottom and each side during a very short interval of time (Δt) is given by:

$$\Delta d' = Q_s \Delta t / [P L(1 - p)] \tag{5.11}$$

in which P is the total perimeter of the breach, L is the length of the breach through the dam, and p is the porosity of the breach material.

Computational algorithm. The sequence of computations in the model are iterative since the flow into the breach is dependent on the bottom elevation of the breach and its width while the breach dimensions are dependent on the erosion depth (Δd) which is dependent on the sediment transport capacity of the breach flow; and the sediment transport capacity is dependent on the breach size and flow. A simple iterative algorithm is used to account for the mutual dependence of the flow, erosion, and breach properties. An estimated incremental erosion depth (Δd) is used at each time step to start the iterative solution. This estimated value can be extrapolated from previously computed values. Convergence occurs when $\Delta d'$, computed from Eq. (5.11), differs from the estimated Δd by less than an

acceptable specified tolerance. Typical applications of the BREACH model require less than a minute on microcomputers. The computations show very little sensitivity to a reasonable variation in the specified time step size. The model is numerically robust, i.e., it has not shown any numerical instability or convergence problems.

Applications. BREACH was applied to the piping initiated failure of the earthfill Teton Dam which breached in June 1976, releasing an estimated peak discharge (Q_p) of 2.2 million cfs having a range of 1.6 to 2.6 million cfs. The simulated breach hydrograph is shown in Fig. 5.2. The computed final top breach width (W) of 645 ft compared well with the observed value of 650 ft. The computed slide slope of the breach was 1:1.06 compared to 1:1.00. The computed time (T_p) to peak flow was 2.2 hr. Additional information on this and another successful application of BREACH to the overtopping failure of a naturally formed landslide dam on the Mantaro river in Peru, which breached in June 1974, can be found elsewhere (Fread, 1984). The model has also been satisfactorily verified with the piping-initiated failure of the 28 ft high Lawn Lake Dam in Colorado (Jarrett and Costa, 1982).

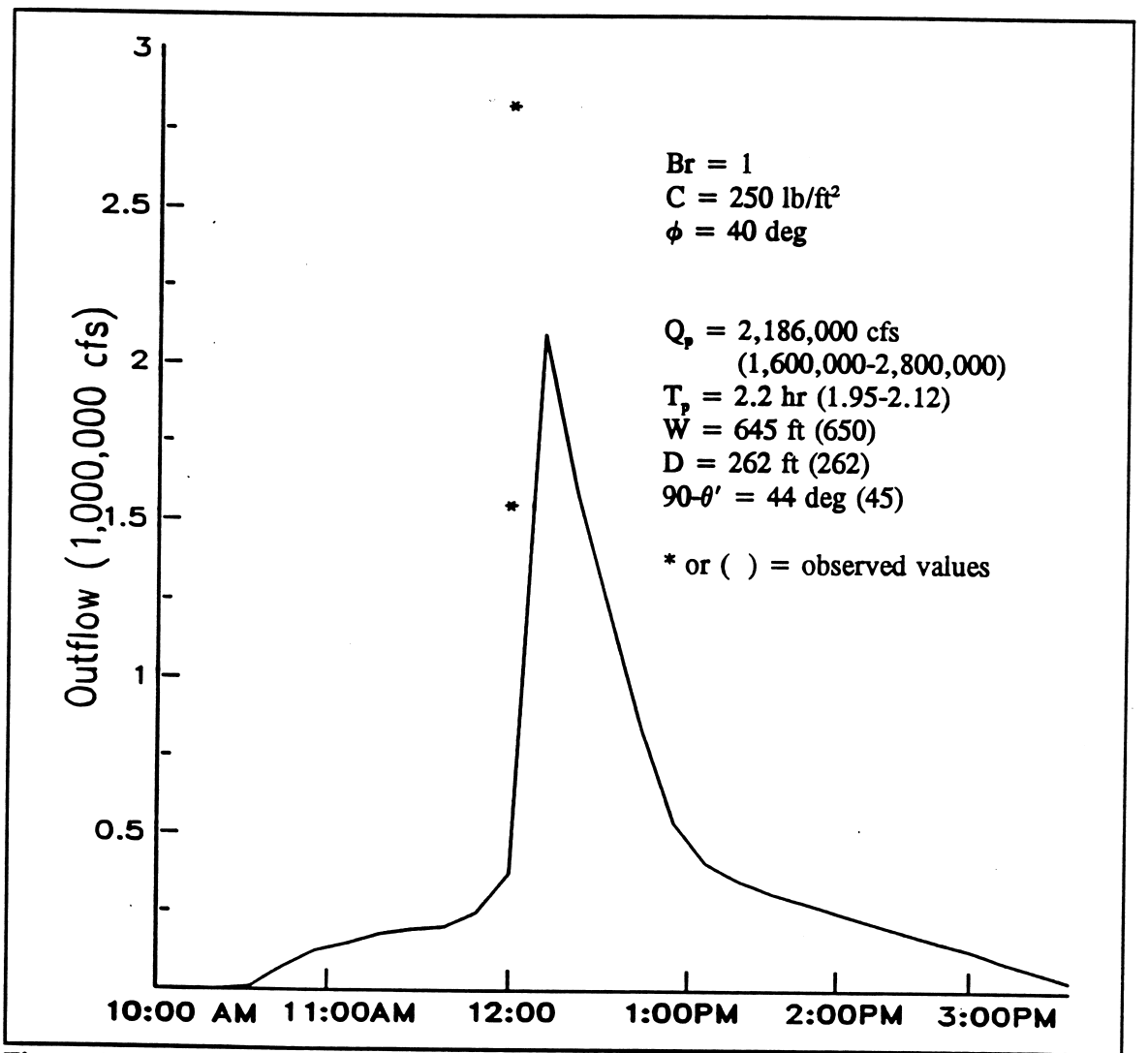

Figure 5.2 Teton Dam: Predicted and observed breach outflow hydrograph and breach properties

5.2.4 Assessment of Breach Parameters

A method for quickly checking the overall reasonableness of the selected breach parameters ($\bar{b}$ and τ) uses the following equations:

$$Q_p^* = 370\ (V_r\ H_d)^{0.5} \tag{5.12}$$

$$Q_p = 3.1\ \bar{b} \left[\frac{C}{\tau + C/\sqrt{H_d}} \right]^3 \tag{5.13}$$

in which Q_p^* and Q_p are the expected peak discharge (cfs) through the breach, V_r and H_d are the reservoir volume (acre-ft) and height (ft) of dam, respectively, and $C = 23.4\ A_r/\bar{b}$ in which A_r is the surface area (acres) of the reservoir at the top of the dam. Eq. (5.12) was developed by Hagen (1982) from historical data of 14 dam failures; it provides a maximum envelope of all 14 of the observed discharges. It over-estimates the peak discharges for each of some 21 observed dam failures (including the previously mentioned 14 failures) by an average of 130 percent. Eq. (5.13) was developed by Fread (1981) and is used in the NWS Simplified Dam Break Model, SMPDBK (Wetmore and Fread, 1984). Eq. (5.13) yields peak discharges within a few percent of those produced by a more exact numerical method based on reservoir level-pool routing described later in Section 5.3.1.5.

After selecting $\bar{b}$ and τ, Eq. (5.13) is used to compute Q_p which then can be compared with Q_p^* from Eq. (5.12). If $Q_p > Q_p^*$, then probably either $\bar{b}$ is too large and/or τ is too small.

Selection of breach parameters introduces a varying degree of uncertainty in the downstream flooding predictions produced by a dam-breach flood model; however, errors in the breach description and thence in the resulting peak outflow rate are damped-out as the flood wave advances downstream, i.e., variations in Q_p due to different breach parameters are reduced as the flood peak advances downstream. The extent of damping is related to the size of the downstream floodplain, i.e., the wider the floodplain, the greater the extent of damping. Sensitivity tests on the breach parameters are best determined using a dam-breach flood model and then comparing the variation in simulated flood peaks at critical downstream locations. In this way, the real uncertainty in the breach parameter selections will be determined.

For conservative predictions which err by creating too large of flood waves, values for b and z should produce an average breach width $\bar{b}$ in the uppermost range of probable values for a certain type of dam. The time of failure (τ) should be selected in the lower range of probable values to produce a maximum outflow.

Also, Eq. (5.13) can be used conveniently to test the sensitivity of $\bar{b}$ and τ for a specific reservoir having properties of V_r, H_d, and A_r. For example, using Eq. (5.13) for a moderately large reservoir (V_r = 250,000 acre-ft, H_d = 250 ft, A_r = 2,000 acres) it can be shown that Q_p varies in proportion to the variation in $\bar{b}$; however, Q_p only varies by less than 1/5 of the variation in τ. Although for a fairly small reservoir (V_r = 500 acre-ft, H_d = 40 ft, A_r = 10 acres), it can be shown, using Eq. (5.13), that Q_p varies less than 20 percent for a variation in $\bar{b}$ of 50 percent; however, Q_p varies about 40 percent for a variation in τ of 50 percent. Thus, it may be generalized, that for large reservoirs Q_p is quite sensitive to $\bar{b}$ and rather insensitive to τ, while for very small reservoirs Q_p is relatively insensitive to $\bar{b}$ and quite sensitive to τ.

5.3. DAM-BREACH FLOOD ROUTING

5.3.1 Dynamic Routing

Flood waves produced by the breaching (failure) of a dam are known as dam-breach flood waves. They are much larger in peak magnitude, considerably more sharp-peaked, and generally of much shorter duration with acceleration components of a far greater significance than flood waves produced by precipitation runoff. The prediction of the extent and time of occurrence of flooding in the downstream valley is known as flood routing. The dam-breach wave is modified (attenuated, lagged, and distorted) as it flows (is routed) through the downstream valley due to the effects of valley storage, frictional resistance to flow, floodwave acceleration components, flow losses, and downstream channel constrictions and/or flow control structures. Modifications to the dam-break flood wave are manifested as attenuation (reduction) of the flood peak magnitude, spreading-out or dispersion of the temporal varying flood-wave volume, and changes in the celerity (propagation speed) or travel time of the flood wave. If the downstream valley contains significant storage volume such as a wide floodplain, the flood wave can be extensively attenuated and its propagation speed greatly reduced. Even when the downstream valley approaches that of a relatively narrow uniform rectangular-shaped section, there is appreciable attenuation of the flood peak and reduction in the wave celerity as the wave progresses through the valley.

There are two basic types of flood routing methods, hydrologic and hydraulic routing. (See Fread (1985, 1992) for a more complete description of the two types of routing methods.) The hydrologic methods usually provide a more approximate analysis of the progression of a flood wave through a river reach than do the hydraulic methods. The hydrologic methods are used for reasons of convenience and economy. They are most appropriate, as far as accuracy is concerned, when the flood wave is not rapidly varying, i.e., the flood-wave acceleration effects are negligible compared to the effects of gravity and channel friction. Also, they are best used when the flood wave is very similar in shape and magnitude to previous flood waves for which stage and discharge observations are available for calibrating the hydrologic routing parameters (coefficients), and when unsteady backwater effects are negligible.

In routing dam-break flood waves, a particular hydraulic routing method known as dynamic routing is most appropriate because of its ability to provide more accuracy in simulating the dam-break flood wave than that provided by the hydrologic methods, as well as, other less complex hydraulic methods such as the kinematic wave and the diffusion wave methods (Fread, 1985, 1992). Of the many available hydrologic and hydraulic routing techniques, only dynamic routing accounts for the acceleration effects associated with the dam-break wave and the influence of downstream unsteady backwater effects produced by channel constrictions, dams, bridge-road embankments, and tributary inflows. Also, dynamic routing can be used economically, i.e., the computational time can be made rather insignificant if advantages of certain "implicit" numerical solution techniques are utilized.

Dynamic routing is based on the complete one-dimensional equations of unsteady flow which are used to route the dam-break flood hydrograph through the downstream valley. The complete one-dimensional equations are an expanded version of the original equations developed by Barré de Saint-Venant (1871). The only coefficient that must be extrapolated beyond the range of past experience is the coefficient of flow resistance. Guidance for the selection and sensitivity of this parameter is discussed later in Sections 5.4.3 and 5.6.3, respectively.

5.3.1.1 Saint-Venant Equations. A modified and expanded form (Fread, 1988, 1992) of the original one-dimensional Saint-Venant equations (Saint-Venant, 1871; Henderson, 1966; Chow et al., 1988) consist of a conservation of mass equation, i.e.,

$$\frac{\partial Q}{\partial x} + \frac{\partial s_c (A + A_o)}{\partial t} - q = 0 \tag{5.14}$$

and the momentum equation, i.e.,

$$\partial(s_m Q)/\partial t + \partial(\beta Q^2/A)/\partial x + gA(\partial h/\partial x + S_f + S_{ce} + S_i) + L + W_f B = 0 \tag{5.15}$$

where h is the water-surface elevation, A is the active cross-sectional area of flow, A_o is the inactive (off-channel storage) cross-sectional area which may be preferred omitted when used to represent heavily wooded floodplains, and its effect represented by a higher frictional resistance for that portion of the cross section, s_c and s_m are area-weighted and conveyance-weighted sinuosity factors, respectively (Delong, 1989) which correct for the departure of a sinuous in-bank channel from the x-axis of the floodplain, x is the longitudinal mean flow-path distance measured along the center of the watercourse (channel and floodplain), t is time, q is the lateral inflow or outflow per lineal distance along the watercourse (inflow is positive and outflow is negative), β is the momentum coefficient for nonuniform velocity distribution within the cross section, g is the gravity acceleration constant, S_f is the boundary friction slope, S_{ce} is the expansion/contraction (large eddy loss) slope, and S_i is the viscous dissipation slope.

Friction slope. The boundary friction slope (S_f) is evaluated from Manning's equation for uniform, steady flow, i.e.,

$$S_f = n^2 |Q| Q/(\mu^2 A^2 R^{4/3}) = |Q| Q/K^2 \tag{5.16}$$

in which n is the Manning coefficient of frictional resistance, R is the hydraulic radius, μ is a units conversion factor (1.49 for US units and 1.0 for SI), and K is the channel conveyance factor. The absolute value of Q is used to correctly account for the possible occurrence of reverse (negative) flows. The conveyance formulation is preferred (for numerical and accuracy considerations) for composite channels having wide, flat overbanks or floodplains in which K represents the sum of the conveyance of the channel (which is corrected for sinuosity effects by dividing by s_m), and the conveyances of left and right floodplain areas.

When the conveyance factor (K) is used to evaluate S_f, the river channel/valley cross-sectional properties are designated as left floodplain, channel, and right floodplain rather than as a composite channel/valley section. Special orientation for designating left or right is not required as long as consistency is maintained. The conveyance factor is evaluated as follows:

$$K_f = \frac{\mu}{n_f} A_f R_f^{2/3} \tag{5.17}$$

$$K_c = \frac{\mu A_c R_c^{2/3}}{n_c s_m^{1/2}} \tag{5.18}$$

$$K_r = \frac{\mu}{n_r} A_r R_r^{2/3} \tag{5.19}$$

$$K = K_\ell + K_c + K_r \tag{5.20}$$

in which the subscripts ℓ, c, and r designate left floodplain, channel, and right floodplain, respectively.

Sinuosity Factors. The area-weighted and conveyance-weighted sinuosity factors (s_c and s_m, respectively) in Eqs. (5.14), (5.15), and (5.18) represent the ratio(s) of the flow-path distance along a meandering channel to the mean flow-path distance along the floodplain. They vary with depth of flow according to the following relations:

$$s_{c_J} = \frac{\sum_{k=2}^{k=J} \Delta A_{\ell_k} + \Delta A_{c_k} s_k + \Delta A_{r_k}}{A_{\ell_J} + A_{c_J} + A_{r_J}} \tag{5.21}$$

$$s_{m_J} = \frac{\sum_{k=2}^{k=J} \Delta K_{\ell_k} + \Delta K_{c_k} s_k + \Delta K_{r_k}}{K_{\ell_J} + K_{c_J} + K_{r_J}} \tag{5.22}$$

in which $\Delta A = A_{J+1} - A_J$, and s_k represents the sinuosity factor for a differential portion of the flow between the J^{th} depth and the $J+1^{th}$ depth, and K is the conveyance factor.

Expansion/contraction effects. The term (S_{ec}) is computed as follows:

$$S_{ec} = k_{ec} \Delta (Q/A)^2 / (2g \Delta x) \tag{5.23}$$

in which k_{ec} is the expansion/contraction coefficient (negative for expansion, positive for contraction) which varies from -1.0/0.4 for an abrupt change in section geometry to -0.3/0.1 for a very gradual, curvilinear transition between cross sections. The Δ represents the difference in the term $(Q/A)^2$ at two adjacent cross sections separated by a distance Δx. If the flow direction changes from downstream to upstream, k_{ec} can be automatically changed (Fread, 1988).

Since dam-break floods usually have much greater velocities, it is important, especially for nonuniform channels (Rajar, 1978) to include in the Saint-Venant momentum Eq. (5.15) the expansion/contraction losses via the S_{ec} term defined by Eq. (5.23). The ratio of expansion/contraction losses (form losses) to the friction losses can be in the range of $0.01 < S_{ec}/S_f < 1.0$. The larger ratios occur for very irregular channels with relatively small n values.

Momentum correction coefficient. The momentum correction coefficient (β) for nonuniform velocity distribution is:

$$\beta = \frac{K_\ell^2/A_\ell + K_c^2/A_c + K_r^2/A_r}{(K_\ell + K_c + K_r)^2/(A_\ell + A_c + A_r)} \tag{5.24}$$

in which K is conveyance, A is wetted area, and the subscripts ℓ, c, and r denote left floodplain, channel, and right floodplain, respectively. When floodplain properties are not separately specified and the total cross section is treated as a composite section, β can be approximated as $1.0 \leq \beta \leq 1.06$ in lieu of Eq. (5.24).

Lateral flow momentum. The term (L) in Eq. (5.15) is the momentum effect of lateral flows, and has the following form: (a) lateral inflow, $L = -qv_x$, where v_x is the velocity of lateral inflow in the x-direction of the main channel flow; (b) seepage lateral outflow, $L = -0.5qQ/A$; and (c) bulk lateral outflow, $L = -qQ/A$ (Strelkoff, 1969).

Mud or debris flows. The term (S_i) is included in the momentum equation (5.15) in addition to S_f to account for viscous dissipation effects of non-Newtonian flows such as mud or debris flows. Mine tailings dams, where the viscous contents retained by the dam have non-Newtonian properties, are dam-breach flood applications requiring the use of S_i in Eq. (5.15). This effect becomes significant only when the solids concentration of the flow is in the range of about 40 to 50 percent by volume. For concentrations of solids greater than about 50 percent, the flow behaves more as a landslide and is not governed by the Saint-Venant equations. S_i is evaluated for any non-Newtonian flow as follows:

$$S_i = \frac{\kappa}{\gamma}\left[\frac{(b+2)Q}{AD^{b+1}} + \frac{(b+2)(\tau_o/\kappa)^b}{2D^b}\right]^{1/b} \qquad (5.25)$$

in which γ is the fluid's unit weight, τ_o is the fluid's yield strength, D is the hydraulic depth (A/B), $b = 1/m$ where m is the exponent of the power function that fits the fluid's stress(τ_s)-strain(dv/dy) properties, and κ is the apparent viscosity or scale factor of the power function, i.e., $\tau_s = \tau_o + \kappa(dv/dy)^m$. The viscous properties, τ_o and κ, can be estimated from the solids concentration ratio of the mud flow (O'Brien and Julien, 1984).

Wind effects. The last term ($W_f B$) in Eq. (5.15) represents the resistance effect of wind on the water surface (Fread, 1985, 1992); B is the wetted topwidth of the active flow portion of the cross section; and $W_f = V_r|V_r|\,c_w$, where the wind velocity relative to the water is $V_r = V_w \cos w + V$, V_w is the velocity of the wind (+) if opposing the flow velocity and (-) if aiding the flow, w is the acute angle the wind direction makes with the x-axis, V is the velocity of the unsteady flow, and c_w is a wind friction coefficient. This modeling capability can be used to simulate the effect of potential dam overtopping due to wind set-up within a reservoir by applying the Saint-Venant equations to the unsteady flow in a reservoir.

5.3.1.2 Implicit Four-Point, Finite-Difference Approximations. The extended Saint-Venant Eqs. (5.14) and (5.15) constitute a system of partial differential equations with two independent variables, x and t, and two dependent variables, h and Q; the remaining terms are either functions of x, t, h, and/or Q, or they are constants. The partial differential equations can be solved numerically by approximating each with a finite-difference algebraic equation; then the system of algebraic equations are solved in conformance with prescribed initial and boundary conditions.

Of various implicit, finite-difference solution schemes that have been developed, a four-point scheme first used by Preissmann (1961) and later a weighted version by many others (Fread, 1974, 1977, 1985, 1988; Cunge et al., 1980) is most advantageous. It is readily used with unequal distance steps, its stability-convergence properties are conveniently modified, and boundary conditions are easily applied.

Space-time plane. In the weighted four-point implicit scheme, the continuous x-t region in which solutions of h and Q are sought is represented by a rectangular grid of discrete points as shown in Fig. 5.3. The x-t plane (solution domain) is a convenient method for expressing relationships among the variables. The grid points are determined by the intersection of lines drawn parallel to the x- and t-axes. Those parallel to the t-axis represent locations of cross sections; they have a spacing of Δx, which need not be the same between each pair of cross sections. Those parallel to the x-axis represent time lines; they have a spacing of Δt, which also need not be the same between successive time lines. Each point in the rectangular network can be identified by a subscript (i) which designates the x-position or cross section and a superscript (j) which designates the particular time line.

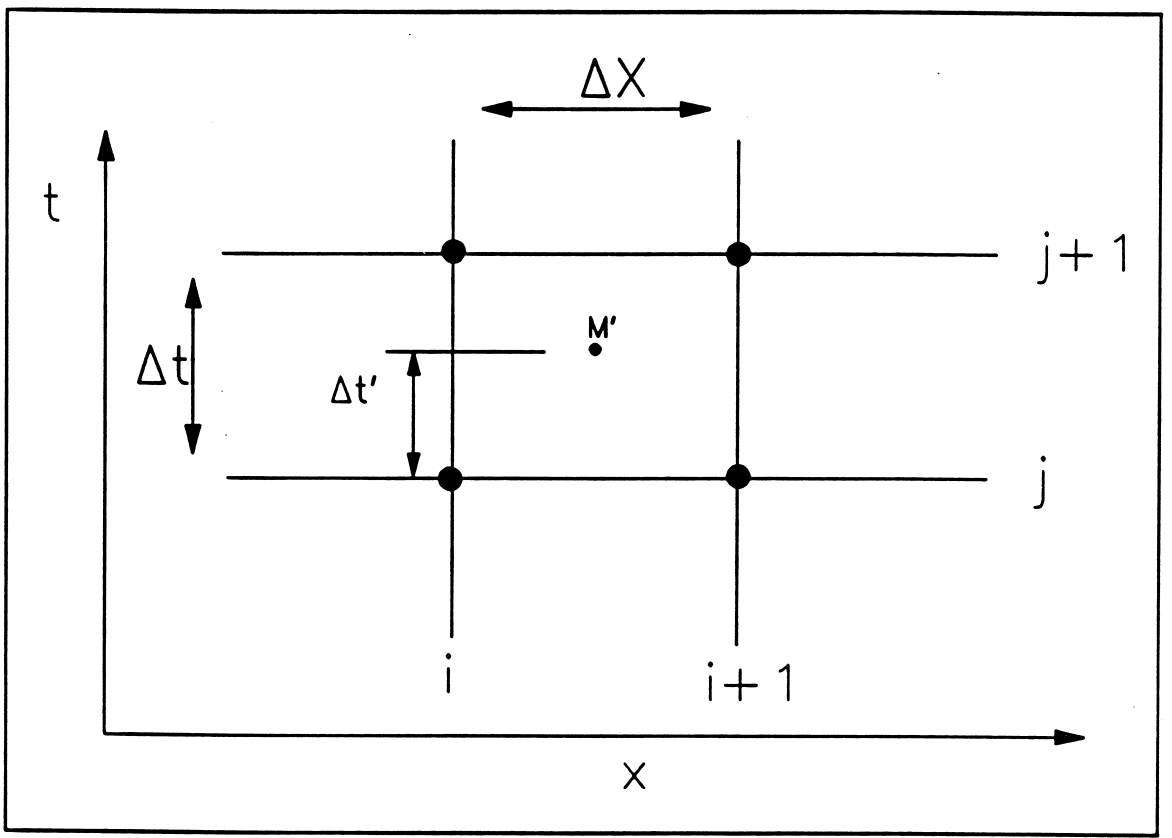

Figure 5.3 The x-t solution domain for the weighted four-point implicit scheme

Numerical approximations. The time derivatives are approximated by a forward-difference quotient at point M′ (Fig. 5.3) centered between the i and i+1 lines along the x-axis, i.e.,

$$\partial\phi/\partial t \simeq (\phi_i^{j+1} + \phi_{i+1}^{j+1} - \phi_i^j - \phi_{i+1}^j)/(2\,\Delta t_j) \qquad (5.26)$$

where ϕ represents any dependent variable or functional quantity (Q, s_c, s_m, A, A_o, q, h). Spatial derivatives are approximated at point M′ by a forward-difference quotient located between two adjacent time lines according to weighting factors of θ (the ratio $\Delta t'/\Delta t$ shown in Fig. 5.3) and $1-\theta$, i.e.,

$$\partial\phi/\partial x \simeq \theta(\phi_{i+1}^{j+1} - \phi_i^{j+1})/\Delta x_i + (1-\theta)(\phi_{i+1}^{j} - \phi_i^{j})/\Delta x_i \quad (5.27)$$

Non-derivative terms are approximated with weighting factors at the same time level (point M') where the spatial derivatives are evaluated, i.e.,

$$\phi \simeq \theta(\phi_i^{j+1} + \phi_{i+1}^{j+1})/2 + (1-\theta)(\phi_i^{j} + \phi_{i+1}^{j})/2 \quad (5.28)$$

Numerical stability. The weighted four-point implicit scheme is unconditionally, linearly stable for $\theta \geq 0.5$ (Fread, 1974); however, the sizes of the Δt and Δx computational steps are limited by the accuracy of the assumed linear variations of functions between the grid points in the x-t solution domain. Values of θ greater than 0.5 dampen parasitic oscillations which have wave lengths of about $2\Delta x$ that can grow enough to invalidate or destroy the solution. The θ weighting factor causes some loss of accuracy as it departs from 0.5, a box scheme, and approaches 1.0, a fully implicit scheme. This effect becomes more pronounced as the magnitude of the ratio $(T_r/\Delta t)$ decreases where T_r is the time of rise of the hydrograph (time interval from beginning of rise to peak of the hydrograph). Usually, a θ weighting factor of 0.60 is used to minimize the loss of accuracy while avoiding the possibility of weak (pseudo) instability for θ values of 0.5 when frictional effects are minimal.

Selection of Δt and Δx computational parameters. The computational time step (Δt) can be either specified or automatically determined to best suit the most rapidly rising hydrograph occurring within the system of rivers containing one or more breaching dams. The time step is selected according to the following:

$$\Delta t = T_r/M \quad (5.29)$$

where T_r is the minimum time of rise of any hydrograph that has been specified at upstream boundaries or in the process of being generated at a breaching dam. M is user specified according to the following guidance (Fread, 1993):

$$M \simeq 2.67\left[1 + \mu' n^{0.9}/(q^{0.1} S_o^{0.45})\right] \quad (5.30)$$

in which $\mu' = 3.97$ (3.13 SI units), n is the Manning friction coefficient, q is the peak flow per unit channel width, and S_o is the channel bottom slope. M usually varies within the range, $6 \leq M \leq 40$, with M often assumed to be approximately 20.

The Δx computational distance step can be specified or automatically determined according to the smaller of two criteria (Fread, 1993). The first criterion is:

$$\Delta x \leq cT_r/20 \quad (5.31)$$

in which c is the bulk wave celerity (the celerity or velocity associated with an essential characteristic of the unsteady flow such as the peak of the hydrograph). In most applications, the wave velocity is well approximated as a kinematic wave, and c is estimated as 3/2V (V is the flow velocity) or c can be obtained by dividing the distance between two points along the channel by the difference in the times of occurrence of the peak of an observed flow hydrograph at each point. Since c can vary along the channel, Δx may not be constant along the channel.

The second criterion for selecting Δx is the restriction imposed by rapidly varying cross-sectional changes along the x-axis of the watercourse. Such expansion/contraction is limited to the following inequality (Samuels, 1985):

$$0.635 < A_{i+1}/A_i < 1.576 \tag{5.32}$$

This condition results in the following approximation for the maximum computational distance step:

$$\Delta x \leq L'/N \tag{5.33}$$

where:

$$N = 1 + 2\,|A_i - A_{i+1}|/\hat{A} \tag{5.34}$$

in which L′ is the distance between two adjacent cross sections differing from one another by approximately 50 percent or greater, A is the active cross-sectional area, i and i+1 are index counters, $\hat{A} = A_{i+1}$ if $A_i > A_{i+1}$ (contracting reach) or $\hat{A} = A_i$ if $A_i < A_{i+1}$ (expanding reach), and N is rounded to the nearest integer value.

Significant changes in the bottom slope of the watercourse also require small distance steps in the vicinity of the change. This is required particularly when the flow changes from subcritical to supercritical or conversely along the watercourse. Such changes can require computational distance steps in the range of 50 to 200 ft.

Automatic interpolation. It is essential for a dam-breach flood routing model to automatically provide linearly interpolated cross sections at a user specified spatial resolution in order to increase the spatial frequency at which solutions to the Saint-Venant equations are obtained. This is often required for purposes of attaining numerical accuracy/stability when (a) routing very sharp-peaked hydrographs such as those generated by breached dams, (b) when adjacent cross sections either expand or contract by more than about 50 percent, and (c) where mixed flow changes from subcritical to supercritical or vice versa.

Algebraic routing equations. Using the finite-difference operators of Eqs. (5.26) to (5.28) to replace the derivatives and other variables in Eqs. (5.14) and (5.15), the following weighted four-point, implicit finite-difference algebraic equations are obtained:

$$\theta\left[\frac{Q_{i+1}^{j+1} - Q_i^{j+1}}{\Delta x_i}\right] - \theta\, q_i^{j+1} + (1-\theta)\left[\frac{Q_{i+1}^{j} - Q_i^{j}}{\Delta x_i}\right] - (1-\theta)\, q_i^{j} + \left[\frac{s_{c_i}^{j+1}(A+A_o)_i^{j+1} + s_{c_i}^{j+1}(A+A_o)_{i+1}^{j+1} - s_{c_i}^{j}(A+A_o)_i^{j} - s_{c_i}^{j}(A+A_o)_{i+1}^{j}}{2\Delta t_j}\right] = 0 \tag{5.35}$$

$$\left[\frac{\left(s_{m_i}Q_i\right)^{j+1} + \left(s_{m_i}Q_{i+1}\right)^{j+1} - \left(s_{m_i}Q_i\right)^{j} - \left(s_{m_i}Q_{i+1}\right)^{j}}{2\Delta t_j}\right] + \theta\left[\frac{(\beta Q^2/A)_{i+1}^{j+1} - (\beta Q^2/A)_i^{j+1}}{\Delta x_i}\right.$$

$$\left. + g\,\bar{A}_i^{j+1}\left[\frac{h_{i+1}^{j+1} - h_i^{j+1}}{\Delta x_i} + \bar{S}_{f_i}^{j+1} + S_{ec_i}^{j+1} + S_{i_i}^{j+1}\right] + L_i^{j+1} + (W_f\bar{B})_i^{j+1}\right] + (1-\theta) \qquad (5.36)$$

$$\left[\frac{(\beta Q^2/A)_{i+1}^{j} - (\beta Q^2/A)_i^{j}}{\Delta x_i} + g\,\bar{A}_i^{j}\left[\frac{h_{i+1}^{j} - h_i^{j}}{\Delta x_i} + \bar{S}_{f_i}^{j} + S_{ec_i}^{j} + S_{i_i}^{j}\right] + L_i^{j} + (W_f\bar{B})_i^{j}\right] = 0$$

where:

$$\bar{A}_i = (A_i + A_{i+1})/2 \qquad (5.37)$$

$$\bar{S}_{f_i} = n^2\,\bar{Q}_i\left|\bar{Q}_i\right|/(\mu^2\,\bar{A}_i^{\,2}\,\bar{R}_i^{4/3}) = \bar{Q}_i\left|\bar{Q}_i\right|/\bar{K}_i^{\,2} \qquad (5.38)$$

$$\bar{Q}_i = (Q_i + Q_{i+1})/2 \qquad (5.39)$$

$$\bar{R}_i \simeq \bar{A}_i/\bar{B}_i \qquad (5.40)$$

$$\bar{B}_i = (B_i + B_{i+1})/2 \qquad (5.41)$$

$$\bar{K}_i = (K_i + K_{i+1})/2 \qquad (5.42)$$

The terms L and W_fB are defined in Eq. (5.15); terms associated with the j^{th} time line are known from initial conditions or previous time-step computations; and μ in Eq. (5.38) is defined in Eq. (5.16). The Δx distance between cross sections is measured along the mean flow path of the (channel/valley) watercourse.

5.3.1.3 Solution Procedure. The flow equations are expressed in finite-difference form for all Δx_i reaches between the first and last (N-th) cross section (i = 1,2,...,N) along the channel/floodplain and then solved simultaneously for the unknowns (Q and h) at each cross section. In essence, the solution technique determines the unknown quantities (Q and h at all specified cross sections along the watercourse) at various times into the future; the solution is advanced from one time to a future time over a finite time interval (time step) of magnitude Δt. Thus, applying Eqs. (5.35) and (5.36) recursively to each of the (N-1) rectangular grids in Fig. 5.3 between the upstream and downstream boundaries, a total of (2N-2) equations with 2N unknowns are formulated. Then, prescribed boundary conditions for subcritical flow (Froude number less than unity, i.e., $Fr = Q/(A\sqrt{gD}) < 1$), one at the upstream boundary and one at the downstream boundary, provide the two additional and necessary equations required for the system to be determinate. Since disturbances can propagate only in the downstream direction in supercritical flow ($Fr > 1$), two upstream boundary conditions and

no downstream boundary condition are required for the system to be determinate. The boundary conditions are described later. Due to the nonlinearity of Eqs. (5.35) and (5.36) with respect to Q and h, an iterative, highly efficient quadratic solution technique such as the Newton-Raphson method is frequently used. Other solution techniques linearize Eqs. (5.35) and (5.36) via a Taylor series expansion or other means. Convergence of the iterative technique is attained when the difference between successive solutions for each unknown is less than a relatively small prescribed tolerance. Convergence for each unknown at all cross sections is usually attained within about one to five iterations. A more complete description of the solution method may be found elsewhere (Fread, 1985).

The solution of 2N x 2N simultaneous equations requires an efficient technique for the implicit method to be feasible. One such procedure requiring 38N computational operations (+, -, *, /) is a compact, penta-diagonal Gaussian elimination method (Fread, 1971, 1985) which makes use of the banded structure of the coefficient matrix of the system of equations. This is essentially the same as the double sweep elimination method (Liggett and Cunge, 1975; Cunge et al., 1980).

When flow is supercritical, the solution technique previously described can be somewhat simplified. Two boundary conditions are required at the upstream boundary and none at the downstream boundary since flow disturbances cannot propagate upstream in supercritical flow. The unknown h and Q at the most upstream cross section are determined from the two boundary equations. Then, cascading from upstream to downstream, Eqs. (5.35) and (5.36) are solved for the two unknowns (h_{i+1} and Q_{i+1}) at each cross section by using Newton-Raphson iteration applied recursively to the two nonlinear equations, Eq. (5.35) and Eq. (5.36).

5.3.1.4 Initial Conditions. Values of water-surface elevation (h) and discharge (Q) for each cross section must be specified initially at time t = 0 to obtain solutions to the Saint-Venant equations. Initial conditions may be obtained from any of the following: (a) observations at gaging stations and interpolated values between gaging stations for intermediate cross sections in large rivers; (b) computed values from a previous unsteady flow solution (used in real-time flood forecasting); and (c) computed values from a steady-flow backwater solution. The backwater method is most commonly used, in which the steady discharge at each cross section is determined by:

$$Q_{i+1} = Q_i + q_i \, \Delta x_i \qquad \ldots \; i = 1,2,3,\ldots,N-1 \tag{5.43}$$

in which Q_1 is the assumed steady flow at the upstream boundary at time t=0, and q_i is the known average lateral inflow or outflow along each Δx reach at t=0. The water-surface elevations (h_i) are computed according to the following steady-flow simplification of the momentum equation, Eq. (5.15):

$$(Q^2/A)_{i+1} - (Q^2/A)_i + g\bar{A}_i \, (h_{i+1} - h_i + \Delta x_i \, \bar{S}_{f_i}) = 0 \tag{5.44}$$

in which $\bar{A}$ and $\bar{S}_{f_i}$ are defined by Eqs. (5.37) and (5.38), respectively. The computations proceed in the upstream direction (i = N-1, ... 3,2,1) for subcritical flow (they must proceed in the downstream direction for supercritical flow). The starting water-surface elevation (h_N) can be specified or obtained from the appropriate downstream boundary condition for the discharge (Q_N) obtained via Eq. (5.43). The Newton-Raphson iterative solution method for a single equation and/or a simple, less efficient, but more stable bi-section iterative technique can be applied to Eq. (5.44) to obtain h_i. The initial water surface profile can also be

obtained from steady-flow backwater models such as HEC-2 (Hydrologic Engineering Center, 1982). Due to friction, small errors in the initial conditions will dampen-out after several computational time steps during the solution of the Saint-Venant equations.

5.3.1.5 Upstream Boundary. Values for the unknowns at external boundaries (the upstream and downstream extremities of the routing reach) of the channel/floodplain, must be specified in order to obtain solutions to the Saint-Venant equations. In fact, in most unsteady flow applications, the unsteady disturbance is introduced at one or both of the external boundaries.

Discharge hydrograph. A specified discharge time series (hydrograph) of inflow to the upstream reservoir is used as the upstream boundary condition. The hydrograph should not be affected by downstream flow conditions. This hydrograph may be obtained from the following: (1) historical observations, (2) assumed design hydrograph, or (3) a runoff hydrograph from specified rainfall-runoff model using calibrated or estimated model parameters. The upstream boundary is expressed mathematically as follows:

$$Q_1^{j+1} - Q(t) = 0 \tag{5.45}$$

in which Q(t) is the specified discharge time series and the subscript indicates the discharge at the first cross section, i.e., the upstream boundary. Eq. (5.45) is used for the upstream boundary if dynamic routing (based on the discretized Saint-Venant equations) commences at this location. However, if the most upstream cross section represents the inlet to an upstream reservoir, a simple routing procedure (reservoir level-pool routing) can be used rather than the considerably more complex dynamic routing if (1) the reservoir is not excessively long and (2) the inflow hydrograph Q(t) is not rapidly changing with time. Level-pool routing errors (E_q), with a magnitude of less than about 5 percent, can usually be tolerated.

Level-pool routing. In level-pool routing, the reservoir is assumed always to have a horizontal (level) water surface throughout its entire length; hence, level-pool. The water-surface elevation (h) changes with time (t), and the outflow from the reservoir is assumed to be a function of h(t). This is the case for reservoirs with uncontrolled overflow spillways such as the ogee-crested, broad-crested weir, and morning-glory types. Gate controlled spillways can be included in level-pool routing if the gate setting (height of the gate bottom above the gate sill) is a predetermined function of time, since the outflow is a function of h and the extent of gate opening. Reservoirs, wherein the dam fails and produces a breach outflow hydrograph, can also be included in the level-pool routing approach.

The upstream boundary condition for this situation is represented by the following expression:

$$Q_1^{j+1} - Q(t) + 43560\ \bar{S}_a\ \Delta h_1^{j+1}/\Delta t^j = 0 \tag{5.46}$$

where:

$$\bar{S}_a = (S_a^j + S_a^{j+1})/2 \tag{5.47}$$

$$\Delta h^{j+1} = h_1^{j+1} - h_1^j \tag{5.48}$$

In this approach, the first cross section is located immediately upstream of the dam, and the second cross section is located immediately downstream of the dam in the tailwater area. Two internal boundary equations (described later) are used to govern the flow through the dam, between the first and second cross sections.

Accuracy of level-pool routing. The accuracy of level-pool routing relative to the more accurate distributed dynamic routing model based on the Saint-Venant equations is shown in Fig. 5.4. The error (in percent) associated with level-pool routing is expressed as a normalized error for the rising limb of the outflow hydrograph. The peak outflow is used as the normalizing parameter. The normalized error (E_q) is:

$$E_q = \frac{100}{Q_{D_p}} \sqrt{\frac{\sum_{i=1}^{N'} \left(Q_{L_i} - Q_{D_i}\right)^2}{N'}} \tag{5.49}$$

in which Q_{L_i} is the level-pool routed flow; Q_{D_i} is the dynamic routed flow peak, and N′ is the number of computed discharges comprising the rising limb of the routed hydrograph. Since level-pool routing is based on the assumption of a horizontal water surface along the length of the reservoir at all times, the error (E_q) associated with level-pool routing increases as (a) reservoir mean depth (D_r) decreases, (b) reservoir length (L_r) increases, (c) time of rise (T_r) of inflow hydrograph decreases, and (d) inflow hydrograph volume decreases. These effects can be represented by three dimensionless parameters, σ_ℓ, σ_t, σ_v; where $\sigma_\ell = D_r/L_r$, $\sigma_t = L_r/[3600\ T_r\ (gD_r)^{1/2}]$ in which g is the gravity acceleration constant and T_r is the time (hrs) from beginning of rise until the peak of the inflow hydrograph, and σ_v = hydrograph volume/reservoir volume. As shown in Fig. 5.4, E_q increases as σ_t increases and as σ_ℓ and σ_v decrease; also the influence of σ_v increases as σ_ℓ decreases. Level-pool routing is not recommended when the inflow hydrograph is one generated from an upstream dam failure.

5.3.1.6 Downstream Boundary. For subcritical flow, a specified discharge or water-surface elevation time series, or a tabular relation between discharge and water-surface elevation (single-valued rating curve) can be used as the downstream boundary condition.

Loop rating. Another downstream boundary condition can be a computed loop-rating curve based on the Manning equation, i.e.,

$$Q_N^{j+1} - \mu/n\ A_N^{j+1}\left(R_N^{j+1}\right)^{2/3}\left(S_{f_N}^{j}\right)^{1/2} = 0 \tag{5.50}$$

The loop is produced by using the friction slope (S_f) rather than the channel bottom slope (S_o) in the Manning equation. The friction slope exceeds the bottom slope during the rising limb of the hydrograph while the reverse is true for the recession limb. The friction slope (S_f) is approximated by using Eq. (5.15) where L and W_f are assumed to be zero while s_m and β are assumed to be unity (Fread, 1985, 1988, 1992), i.e.,

$$S_{f_N}^{j} \simeq -\left(Q_N^{j} - Q_N^{j-1}\right)/\left(gA_N^{j}\,\Delta t^{j}\right) - \left[(Q^2/A)_N^{j} - (Q^2/A)_{N-1}^{j}\right]/\left(gA_N^{j}\,\Delta x_{N-1}\right) - \left(h_N^{j} - h_{N-1}^{j}\right)/\Delta x_{N-1} \tag{5.51}$$

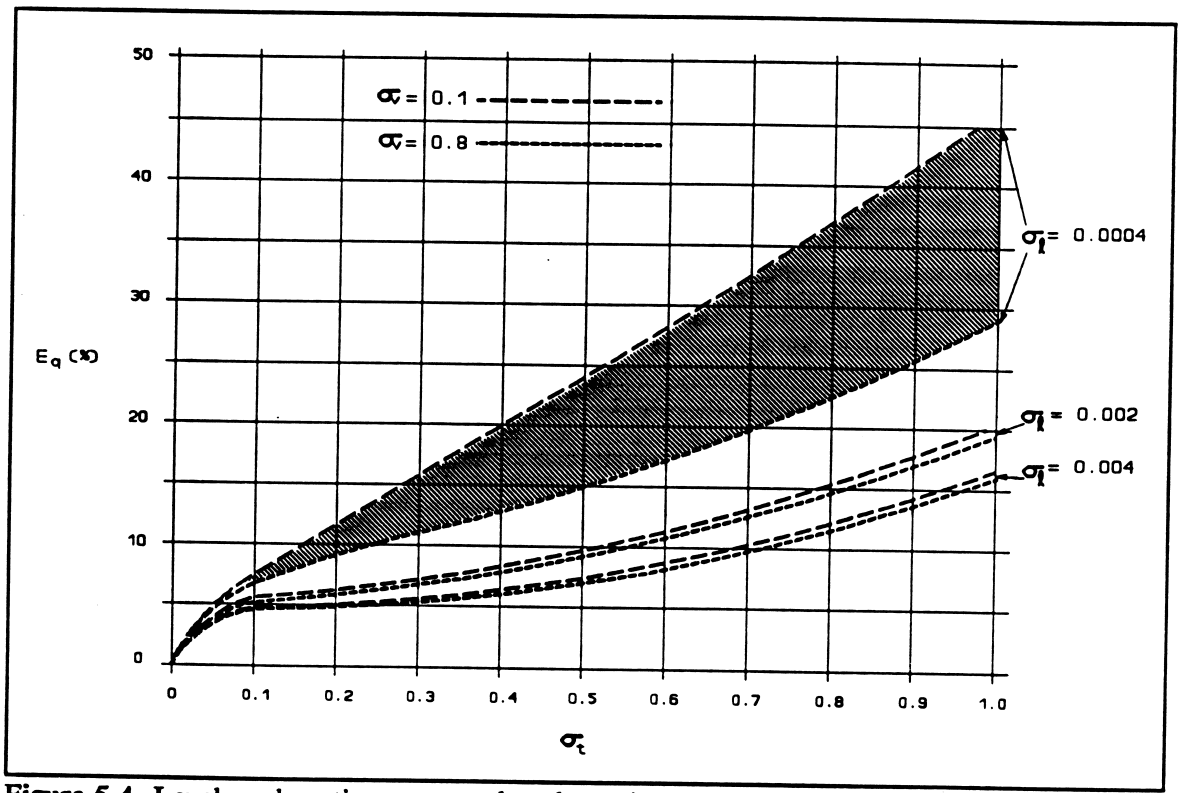

Figure 5.4 Level-pool routing compared to dynamic routing showing the normalized error (E_q) of the outflow hydrograph as a function of dimensionless parameters σ_t, σ_t, and σ_v

The loop-rating boundary equation allows the unsteady wave to pass the downstream boundary with minimal disturbance by the boundary itself, which is desirable when the routing is terminated at an arbitrary location along the channel/floodplain and not at a location of actual flow control such as a dam or waterfall, or where the flow is affected by downstream backwater conditions produced by tidal action, reservoirs, or tributary inflow.

Critical flow. The downstream boundary condition can also be a critical flow section such as the entrance to a waterfall or a steep channel reach, i.e.,

$$Q_N^{j+1} - \sqrt{g/B_N^{j+1}} \left(A_N^{j+1}\right)^{3/2} = 0 \qquad (5.52)$$

Critical flow occurs when the bottom slope (S_o) equals or exceeds the critical slope (S_c) which can be easily computed as follows:

$$S_c = \hat{\mu}\, n^2/D^{1/3} \qquad (5.53)$$

where $\hat{\mu} = 14.6$ for US units and $\hat{\mu} = 9.8$ for SI units.

Rating curve. When the downstream boundary is a stage/discharge relation (rating curve), the flow at the boundary should not be otherwise affected by flow conditions further downstream. Although there are often some minor effects due to the presence of cross-sectional irregularities downstream of the chosen boundary location, these usually can be neglected unless the irregularity is so pronounced as to cause significant backwater or

drawdown effects. Reservoirs, major tributaries, or tidal effects located below the downstream boundary which cause backwater effects at the boundary should be avoided. When either of these situations are unavoidable, the routing reach should be extended downstream to the dam in the case of the reservoir or to a location downstream of where the major tributary enters. Sometimes the routing reach may be shortened by moving the downstream boundary to a location further upstream where backwater effects are negligible.

5.3.1.7 Internal Boundaries. Often along the channel/floodplain, there are locations such as a dam, bridge, or waterfall (short rapids) where the flow is rapidly varied in space rather than gradually varied. At such locations (internal boundaries), the Saint-Venant equations are not applicable since gradually varied flow is a necessary condition for their derivation. Empirical water elevation-discharge relations such as weir-flow are utilized for simulating rapidly varying flow. At internal boundaries, cross sections are specified for the upstream and downstream extremities of the section where rapidly varying flow occurs. The Δx reach containing an internal boundary requires two internal boundary equations; since, as with any other Δx reach, two equations equivalent to the Saint-Venant equations are required. One of the required internal boundary equations represents conservation of mass with negligible time-dependent storage, i.e.,

$$Q_i^{j+1} - Q_{i+1}^{j+1} = 0 \tag{5.54}$$

Dam. The second equation is usually an empirical rapidly varied flow relation . If the internal boundary represents a dam, the following equation can be used:

$$Q_i^{j+1} - (Q_s + Q_b)^{j+1} = 0 \tag{5.55}$$

in which Q_s and Q_b are the spillway and dam-breach flow, respectively. In this way, the flows Q_i and Q_{i+1} and the elevations h_i and h_{i+1} are in balance with the other flows and elevations occurring simultaneously throughout the entire flow system which may consist of additional downstream dams which are treated as additional internal boundary conditions via Eqs. (5.54) and (5.55). In fact, this approach can be used to simulate the progression of a dam-break flood through an unlimited number of reservoirs located sequentially along the valley. The downstream dams may also breach if they are sufficiently overtopped. The spillway flow (Q_s) is computed from the following expression:

$$Q_s = c_s L_s (h_i - h_s)^{1.5} + c_g A_g (h_i - h_g)^{0.5} + c_d L_d (h_i - h_d)^{1.5} + Q_t \tag{5.56}$$

in which c_s is the uncontrolled spillway discharge coefficient, h_s is the uncontrolled spillway crest, c_g is the gated spillway discharge coefficient, h_g is the center-line elevation of the gated spillway, c_d is the discharge coefficient for flow over the crest of the dam, L_s is the spillway length, and Q_t is a constant outflow term which is head independent or it may be a specified discharge time series. The uncontrolled spillway flow or the gated spillway flow can also be represented as a table of head-discharge values. The gate flow may also be specified as a function of time via a known time series for $A_g(t)$. The breach outflow (Q_b) is computed as broad-crested weir flow (Fread, 1977, 1985, 1988, 1992; Fread and Lewis, 1988), i.e.,

$$Q_b = c_v k_s [3.1\, b_i\, (h_i - h_b)^{1.5} + 2.45\, z\, (h_i - h_b)^{2.5}] \tag{5.57}$$

in which c_v is a small correction for velocity of approach, b_i is the instantaneous breach bottom width, h_i is the elevation of the water surface just upstream of the structure, h_b is the elevation of the breach bottom as described by Eq. (5.2) in which h_b is assumed to be a linear function of time (t_b) from beginning of the breach formation time (τ), z is the side slope of the breach, and k_s is the submergence correction factor due to the downstream tailwater elevation (h_t), i.e.,

$$k_s = 1.0 \qquad h^* \leq 0.67 \tag{5.58}$$

$$k_s = 1.0 - 22.3(h^* - 0.67)^3 \qquad h^* > 0.67 \tag{5.59}$$

where:

$$h^* = (h_t - h_b)/(h_i - h_b) \tag{5.60}$$

If the breach is formed by piping, Eq. (5.57) is replaced by an orifice equation:

$$Q_b = 4.8\ A_p(h_i - h_p)^{1/2} \tag{5.61}$$

where:

$$A_p = [b_i + z(h_p - h_b)](h_p - h_b) \tag{5.62}$$

in which h_p is the specified center-line elevation of the pipe. Each of the terms in Eq. (5.56) may be modified by a submergence correction factor similar to k_s which can be computed by Eq. (5.59) in which h_b is replaced by h_s, h_g, and h_d, respectively.

Bridge. If the internal boundary represents highway/railway bridges together with their earthen embankments which cross the floodplain, Eqs. (5.54) and (5.55) can still be used although Q_s in Eq. (5.55) is computed by the following contracted bridge flow expression:

$$Q_s = C_b\sqrt{g}\ A_{i+1}(h_i - h_{i+1})^{0.5} + C_d k_s(h_i - h_c)^{1.5} \tag{5.63}$$

in which C_b is a coefficient of bridge flow, C_d is the coefficient of flow over the crest of the road embankment, h_c is the crest elevation of the embankment, and k_s is similar to Eqs. (5.58)-(5.60) except h_b is replaced by h_c. A breach of the embankment is treated the same as with dams.

5.3.1.8 Levee Overtopping/Floodplain Interactions. Flows which overtop levees located along either or both sides of a main-stem river and/or its principal tributaries can be treated as lateral flow (q) in Eqs. (5.14)-(5.15) where the lateral flow diverted over the levee is computed as broad-crested weir flow. This overtopping flow is corrected for submergence effects if the floodplain water-surface elevation sufficiently exceeds the levee crest elevation. After the flood peak passes, the overtopping flow may reverse its direction when the floodplain water-surface elevation exceeds the river water-surface elevation, thus allowing flow to return to the river. The overtopping broad-crested weir flow is computed according to the following:

$$q = -c_f\, k_s\, (h - h_c)^{3/2} \qquad (5.64)$$

where k_s, the submergence correction factor, is computed as in Eqs. (5.58)-(5.60) except $h^* = (h_{fp} - h_c) / (h - h_c)$, in which c_f is the weir discharge coefficient, h_c is the levee-crest elevation, h is the water-surface elevation of the river, and h_{fp} is the water-surface elevation of the floodplain. Flow in the floodplain can affect overtopping flows via the submergence correction factor. Flow may also pass from the waterway to the floodplain through a time-dependent crevasse (breach) in the levee via a breach-flow equation similar to Eq. (5.57). The floodplain, which is separated from the principal routing channel (river) by the levee, may be treated as: (a) a dead-storage area (A_s) in the Saint-Venant equations; (b) a tributary which receives its inflow as lateral flows (the flows from the river which overtop the levee-crest) which are simultaneously dynamically routed along the floodplain; and (c) the flows and water-surface elevations can be computed by using a level-pool routing method particularly if the floodplain is divided into compartments by levees (dikes) or elevated roadways located somewhat perpendicular to the river levee(s).

5.3.1.9 Supercritical/Subcritical Mixed Flow. Flow can change with either time or distance along the routing reach from supercritical to subcritical while passing through critical flow, or conversely. This "mixed flow" requires special treatment to prevent numerical instabilities in the solution of the Saint-Venant equations. This difficulty can be addressed by using a concept based on avoiding the use of the Saint-Venant equations at the point where mixed flow occurs. An enhanced mixed flow algorithm automatically subdivides the total routing reach into sub-reaches wherein only subcritical or supercritical flows occur (Fread, 1983, 1985, 1988). The transition locations where flow changes from subcritical to supercritical or vice versa are treated as boundary conditions thus avoiding the application of the Saint-Venant equations to the transition flow and subsequent numerical solution difficulties. The mixed-flow algorithm has two components, one for obtaining the initial condition of discharge and water elevation at t=0 and another which functions during the unsteady flow solution. The Froude number (Fr) is used to determine the supercritical reaches, for which Fr > 1. At each time step, the solution commences with the most upstream sub-reach, and proceeds sub-reach by sub-reach in the downstream direction. Hydraulic jumps are allowed to move upstream (downstream) at the end of a time step according to the relative values of supercritical (subcritical) sequent depth and the adjacent downstream subcritical (upstream supercritical) depth.

An alternative for treating mixed flows (Fread, et al., 1996) is to provide a "local partial inertia" filter ($1-Fr^m$) which multiplies the first two (inertia) terms in the momentum Eq. (5.15). Fr is the Froude number of the flow in any i^{th} Δx reach and the exponent (m) varies from 1 to 10, with 5 usually preferred. The filter takes on a value of zero when Fr > 1. The local partial inertia filter avoids numerical difficulties associated with mixed flows while introducing negligible errors, less than about 2 percent for almost all flow conditions.

5.3.1.10 Flow Through a River System. A river system consisting of a main-stem river and one or more principal tributaries is efficiently solved using an iterative relaxation method (Fread, 1973, 1985) in which the flow at the confluence of the main-stem and tributary is treated as the lateral inflow/outflow (q) in Eqs. (5.14)-(5.15). If the river consists of bifurcations such as islands and/or complex dendritic systems with tributaries connected to tributaries, etc., a network solution technique is used (Fread, 1985), wherein three internal boundary equations conserve mass and momentum at the confluence. This system of algebraic equations uses a special sparse matrix Gaussian elimination technique for an efficient solution (Fread, 1983).

5.4. DAM-BREACH FLOOD ROUTING DATA

5.4.1 Cross-Sectional Properties

Much of the uniqueness of a specific dam-breach flood routing application is due to the properties of the cross sections located at selected points along the downstream channel/valley shown in Fig. 5.5. The computation of discharge (Q) and water surface elevation (h) by solving the Saint-Venant equations occurs at the locations where cross sections are selected.

5.4.1.1 Active Sections. That portion of the channel cross section in which flow occurs is called active. Cross sections may be of regular or irregular geometrical shape. As indicated in Fig. 5.5, each cross section can be described by tabular values of channel topwidth and water-surface elevation which constitute a piece-wise linear relationship. Generally about 4 to 12 sets of topwidths and associated elevations provide a sufficiently accurate description of the cross section. Area-elevation tables can be generated initially from the specified topwidth-elevation data. Areas or widths associated with a particular water-surface elevation are linearly interpolated from the tabular values. Cross sections at gaging station locations are generally used as computational points, as well as those locations along the river where significant cross-sectional or flow-resistance changes occur or at locations where major tributaries enter. The spacing of cross sections can range from a few hundred feet to a few miles apart. Typically, cross sections are spaced farther apart for large rivers than for small streams, since the degree of variation in the cross-sectional characteristics is greater for the small streams. It is essential that the selected cross sections, with the assumption of linear variation between adjacent sections, represent the volume available to contain the flow along the watercourse.

5.4.1.2 Inactive (Dead) Sections. There can be inactive portions of a cross section where the flow velocity in the x-direction is negligible relative to the velocity in the active portion. The inactive portion is also called off-channel (dead) storage; it is represented by the term (A_o) in Eq. (5.14). Off-channel storage areas can be used to effectively account for adjacent embayments, ravines, or tributaries (see Fig. 5.5) which connect at some elevation with the flow channel but do not convey flow in the x-direction; they serve only to store some of the passing flow. Sometimes, off-channel storage can be used to simulate a heavily wooded floodplain which primarily stores some of the flood waters while conveying a very minimal portion of the flow. Dead storage cross-sectional properties can be described by width (dead storage) vs. elevation tables.

5.4.2 Sinuosity Factors

A meandering or sinuous channel provides a longer flow path than that provided by the floodplain. This effect is simulated via the sinuosity factors (s_c and s_m) in Eqs. (5.14)-(5.15). The sinuosity factor is specified for each reach between two adjacent specified cross sections. The sinuosity factor, which is always ≥ 1.0, is the ratio of the flow-path distance along the meandering channel to the mean flow-path distance along the floodplain. For those elevations used to describe the topwidth at bankfull elevation and below, the sinuosity factor is as previously defined; however, at elevations above bankfull, the sinuosity factor for each layer of flow between specified elevations is decreased such that for those flow layers, say 5 to 10 feet above bankfull, the sinuosity factor is reduced to unity. This indicates that the floodplain flow has fully captured the upper layers of flow directly above the channel.

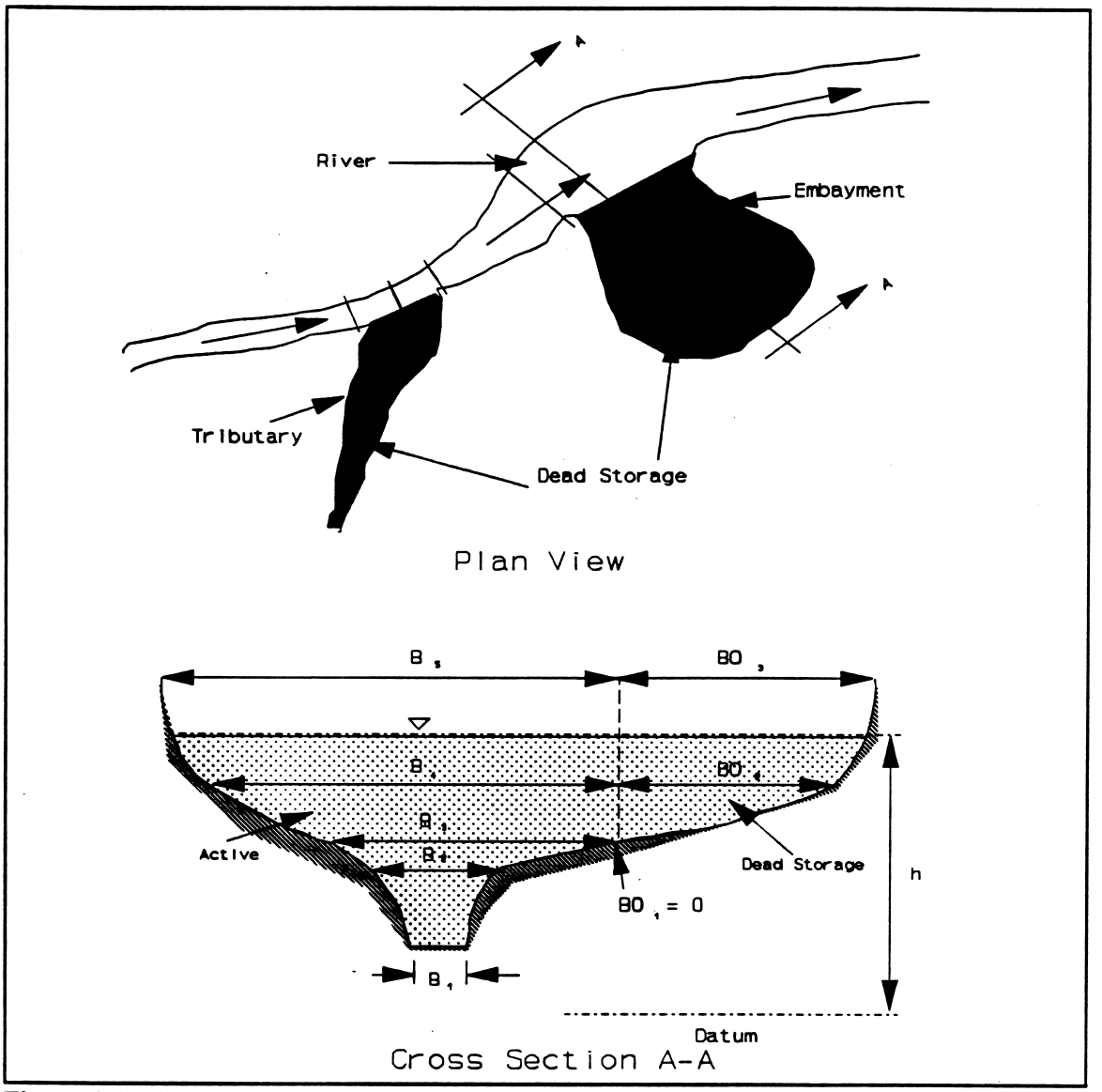

Figure 5.5 Plan view of river with active and dead storage areas, and cross section view

The sinuosity factor, as used in the finite-difference Saint-Venant Eqs. (5.35)-(5.36), is depth-weighted according to Eqs. (5.21)-(5.22). The depth-weighting results in a sinuosity factor which only approaches unity, even for the upper elevations associated with large floodplain flows. This occurs since the total flow is still comprised of the relatively small flow within bankfull which follows the meandering channel, as well as the larger portion of the total flow which follows the floodplain flow path.

5.4.3 Manning n Friction Coefficients

The resistance to flow in the channel/valley may be parameterized by the Manning n or some other friction (roughness) coefficient which represents the effect of roughness elements of the channel bank and bed particles as well as form losses attributed to dynamic alluvial bed-forms and vegetation of various types (grass, shrubs, field crops, brush, and trees) located along the banks and overbanks (floodplain). Also river bend losses are often included as components

of the Manning n. The Manning n is defined for each channel reach and specified as a tabular piece-wise linear function of stage or discharge, with linear interpolation used to obtain values intermediate to the tabulated values.

5.4.3.1 Estimation. The Manning n varies with the magnitude of flow. As the flow increases and more portions of the bank and overbank become inundated, the vegetation located at these elevations causes an increase in the resistance to flow. Also, the Manning n may be larger for small floodplain depths than for larger depths due to flattening of the brush, thick weeds, or tall grass as the flow depths and velocities increase. This effect may be reversed in the case of wooded overbanks where, at the greater depths, the flow impinges against the leaved branches rather than only against the tree trunks, thus increasing the Manning n. The Manning n may also decrease with increasing discharge when the increase in the overbank flow area is relatively small compared to the increase of flow area within the banks, as the case of wide rivers with levees situated closely along the natural river banks, or when floods remain confined within the channel banks. Seasonal influences (leaves and weeds occur in summer but not in winter) may also affect the selection of the Manning n.

Basic references for selecting the Manning n may be found in Chow (1959), Barnes (1967), and Chow et al. (1988); Arcement and Schneider (1984) can be used for wooded and urbanized floodplains; and Jarrett (1984) proposed the following predictor for the Manning n for in-bank flows of relatively steep ($0.002 \leq S_o \leq 0.040$) streams with gravel/cobble/boulder beds, i.e.,

$$n = 0.39\, S_o^{0.38}/R^{0.16} \tag{5.65}$$

in which S_o is the bottom slope (ft/ft) and R is the hydraulic radius (ft). Manning n values for flows less than bankfull are approximately 0.015 - 0.035 for large rivers (Mississippi, Ohio, Missouri, Illinois), 0.03 - 0.04 for moderate sized rivers and streams, 0.04 - 0.07 for mountain streams, and 0.04 - 0.25 for overbank flows (Fread, 1989a).

Unfortunately, the flow observations used in developing the Manning n predictive methodologies have been confined to floods originating from rainfall/snowmelt-runoff. The much greater magnitude of a dam-break flood produces greater velocities and results in the inundation of portions of the floodplain never before inundated.

Also, the dam-break flood is much more capable than the lesser runoff-generated flood of creating and transporting large amounts of debris, e.g., uprooted trees, demolished houses, vehicles, etc. The higher velocities of the dam-breach flood will cause additional energy losses due to temporary flow obstructions formed by transported debris which impinge against some more permanent feature along the river such as a bridge or other man-made structure. Therefore, the Manning n values often need to be increased in order to account for the additional energy losses associated with the dam-break flows such as those due to the temporary debris dams which form and then disintegrate when ponded water depths become too great. The extent of the debris effects, of course, is dependent on the availability and amount of debris which can be transported and the existence of man-made or natural constrictions where the debris may impinge behind and form temporary obstructions to the flow.

5.4.3.2 Calibration. The Manning n for the range of flows associated with previously observed floods may be selected via a trial-and-error calibration methodology. With observed stages and flows, preferably continuous hydrographs from a previous large flood, an unsteady flow routing model can be used to determine the Manning n values as follows: (1) use the observed flow hydrograph as the upstream boundary condition and select an appropriate

downstream boundary (an observed stage hydrograph at the downstream boundary could be used if available); (2) estimate the Manning n values throughout the routing reach; (3) obtain computed h and Q from the solution of the Saint-Venant equations; (4) compare the computed elevations with the observed elevations at the upstream boundary and elsewhere; (5) if the computed elevations are lower than the observed, increase the estimated Manning n values; or if the computed elevations are higher than the observed, decrease the estimated Manning n values; (6) repeat steps (3)-(5) until the computed and observed elevations are approximately the same. The final Manning n values are sufficient for the range of flows used in the calibration; however, the Manning n values for those flow elevations exceeding the observed must be estimated as previously discussed. The calibrated Manning n values, however, provide an initial estimate from which the unknown Manning n values may be extrapolated or ultimately approximated.

5.4.4 Levee Properties

The levee properties required for modeling their effects are the elevation (h_c) of the top of the levee and an estimated discharge coefficient (c_t) which has the range, $2.6 < c_t < 3.1$. These properties need to be specified for each reach between selected cross sections.

5.4.5 Lateral Flows

Specified unsteady flows associated with tributaries that are not dynamically routed can be added to the unsteady flow along the routing reach. This is accomplished via the term q in Eqs. (5.14) and (5.15). The total tributary flow which is a known function of time, i.e., $Q_i(t)$ which is a specified time series, is distributed along a single Δx_i reach, i.e., $q_i(t) = Q_i(t)/\Delta x_i$. Backwater effects of the routed flow on the tributary flow are ignored, and the lateral flow is usually assumed to enter perpendicular to the routed flow. Known outflows can be simulated by using a negative sign with the specified $Q_i(t)$. Numerical difficulties in solving the Saint-Venant equations sometimes arise when the ratio of lateral inflow to channel flow, q_i/Q_i, is too large; this can be overcome by increasing Δx_i for this reach.

5.5. TETON DAM-BREACH FLOOD CASE STUDY

A case study using the DAMBRK Model (Fread, 1977, 1988, 1989; Chow et al., 1988) for the Teton dam-breach flood is presented. The DAMBRK Model is based on the dam breach and flood routing equations presented previously in Sections 5.2 and 5.3. It has been favorably reviewed (Land, 1980; Wurbs, 1986) and has received wide applications in the United States and in many countries throughout the world. DAMBRK model results are compared with observed downstream peak stages, discharges, and travel times.

The Teton Dam, a 300 ft high earthen dam with a 3,000 ft long crest and 250,000 acre-ft of stored water, failed on June 5, 1976, killing 11 people, making 25,000 homeless, and inflicting about $400 million in damages to the downstream Teton-Snake River Valley. Data from a U.S. Geological Survey Report by Ray, et al. (1977) provided observations on the approximate development of the breach, a description of the reservoir storage, downstream cross sections and estimates of Manning n approximately every 5 miles, indirect peak discharge measurements at two sites and rating curves at two other sites, flood-peak travel times, and flood-peak elevations at frequent locations along the downstream channel/valley. The inundated area was as much as 9 miles in width about 16 miles downstream of the dam.

The following breach parameters were used to reconstitute the downstream flooding due to the failure of the Teton Dam: τ = 1.4 hrs, b = 81 ft, z = 1.04, h_{bm} = 0.0, $h_d = H_d$ = 261.5 ft. They were obtained from the BREACH model (Fread, 1984, 1989b). The time of failure (τ) was obtained by using the average of two values, i.e.,

$$\tau = 0.5(\tau_1 + \tau_2) \tag{5.66}$$

where τ_1 is computed by rearranging Eq. (5.13) with Q_p, $\bar{b}$, H_d computed by the BREACH model, i.e.,

$$\tau_1 = C\left[(3.1\ \bar{b}/Q_p)^{1/3} - 1/H_d^{0.5}\right] \tag{5.67}$$

in which Q_p = 2,200,000 cfs, $\bar{b}$ = 353 ft, and C = 2.34 $S_a/\bar{b}$, in which S_a = 1936 acres. The term (τ_2) is derived by equating the integrated area of the computed outflow hydrograph Q(t) (from beginning of breach to T_p, the time when the peak outflow occurs) to a triangle with Q_p as the peak and τ_2 as the base, i.e.,

$$\tau_2 = \frac{2}{Q_p}\int_0^{T_p} Q(t)\,dt \tag{5.68}$$

Cross-sectional properties were used at 12 locations along the 60-mile reach of the Teton-Snake River Valley below the dam. Five topwidths were used to describe each cross section. The downstream valley consisted of a narrow canyon (approx. 1,000 ft wide) for the first 5 miles and thereafter a wide valley which was inundated to a maximum width of about 9 miles. Manning n values ranging from 0.038 to 0.047 were provided from field estimates by the Geological Survey. Computational distance steps (Δx) between cross sections were assigned values that gradually increased from 0.5 miles near the dam, to a value of 1.4 miles near the downstream boundary at the Shelly gaging station (valley mile 59.5 downstream from the dam). The reservoir surface area-elevation values were obtained from U.S. Geological Survey topographic maps. The downstream boundary was assumed to be channel flow control as represented by a loop-rating curve given by Eq. 5.50.

The computed outflow hydrograph using reservoir level-pool routing is shown as the solid line in Fig. 5.6 with a peak value of 2,172,000 cfs, a time to peak of 2.15 hrs, and a total duration of significant outflow of about 6 hrs. This peak discharge is about 30 times greater than the flood of record approximately 45 miles downstream at Idaho Falls on the Snake River. The temporal variation of the computed time-integrated outflow volume compared within 3 percent of the observed. Also, in Fig. 5.6, a comparison is presented of Teton reservoir outflow hydrographs computed via reservoir dynamic routing as shown by the dashed line. Since the breach of the Teton Dam formed gradually over approximately a two hour interval, a steep negative wave did not develop in the reservoir. Also, the inflow to the reservoir was insignificant. For these reasons, the reservoir surface remained essentially level during the reservoir drawdown and the dynamic routing yielded almost the same outflow hydrograph as the level-pool routing technique.

The computed peak discharge values along the 60-mile downstream valley are shown in Fig. 5.7 along with four observed values (two by indirect measurement; two by rating curves) at downstream miles 2.0, 8.5, 43.0, and 59.5. The average absolute difference between the computed and observed values is 5.2 percent. Most apparent is the extreme attenuation of the peak discharge as the flood wave propagates through the valley. Two computed curves are

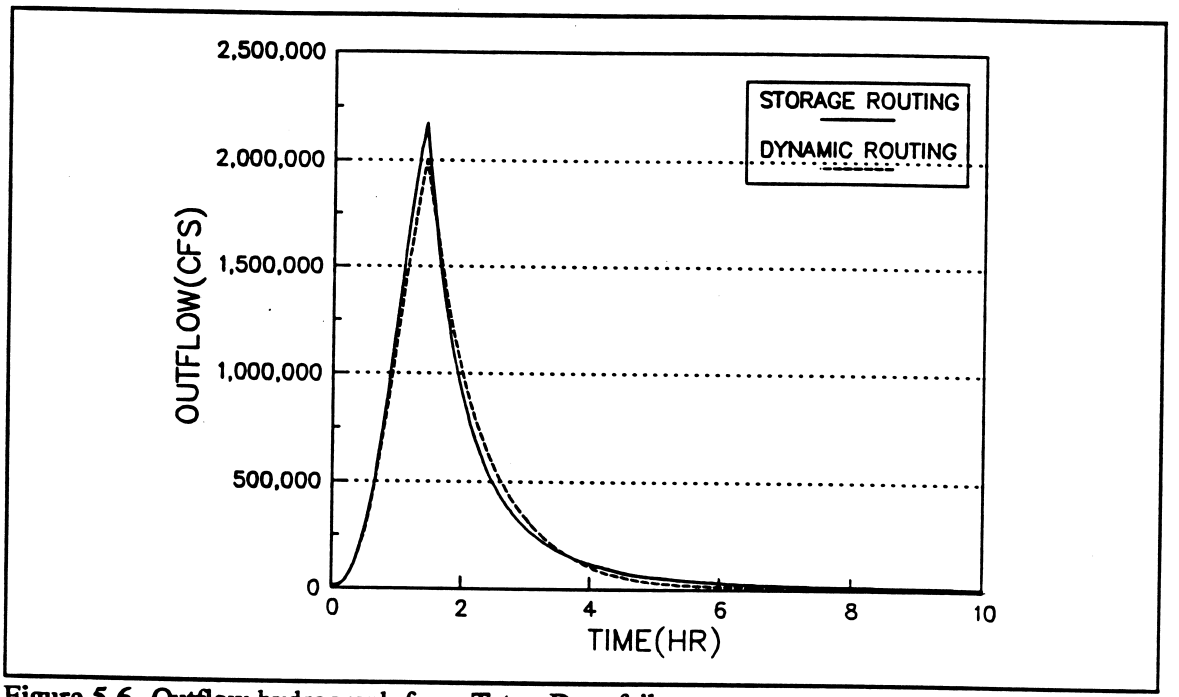

Figure 5.6 Outflow hydrograph from Teton Dam failure

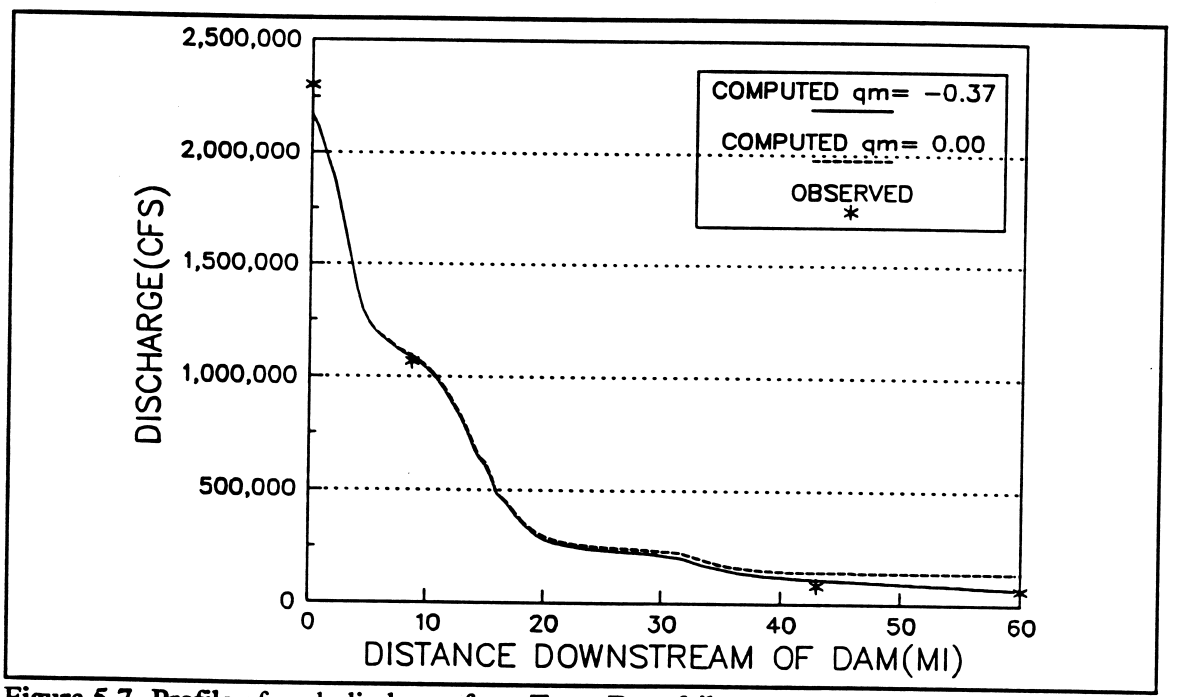

Figure 5.7 Profile of peak discharge from Teton Dam failure

shown in Fig. 5.7; one in which no flow losses were assumed, and a second in which the flow losses amounting to about 30 percent of the reservoir outflow volume, which were due to infiltration and detention storage behind irrigation levees distributed throughout large portions of the inundated floodplain, were accounted for in the routing via the q term in Eqs. (5.14)-(5.15).

The a priori selections of the breach parameters (τ and b) cause the greatest uncertainty in forecasting dam-break flood waves. The sensitivity of downstream peak discharges to reasonable variations in τ and b are shown in Fig. 5.8. Although there are large differences in the discharges (+75 to -42 percent) near the dam, these rapidly diminish in the downstream direction. After 8.5 miles the variation is about ± 17 percent, and after 22 miles the variation has further diminished to about ± 6 percent. The tendency for extreme peak attenuation and rapid damping of differences in the peak discharge is accentuated in the case of Teton Dam due to the presence of the very wide downstream valley. Had the narrow canyon extended all along the 60-mile reach to Shelly, the peak discharge would not have attenuated as much and the differences in peak discharges due to variations in τ and $\bar{b}$ would be more persistent. In this instance, the peak discharge would have attenuated to about 750,000 rather than 67,000 as shown in Fig. 5.8, and the differences in peak discharges at mile 59.5 would have been about ± 17 percent as opposed to ± 5 percent as shown in Fig. 5.8.

Computed peak elevations compared favorably with observed values, as shown in Fig. 5.9. The average absolute error was 1.9 ft, while the average arithmetic error was only +0.8 ft.

The computed flood-peak travel times and three observed values are shown in Fig. 5.10. The differences between the computed and observed travel times at mile 59.5 are about 5 percent for the case of using the estimated Manning n values and about 13 percent if the Manning n values are arbitrarily increased by 20 percent.

As stated previously in Section 5.4.3.1, the Manning n must be estimated, especially for the flows above the flood of record. The sensitivity of the computed water elevations and discharges of the Teton flood due to a substantial change (20 percent) in the Manning n was found to be as follows: (1) 0.3 ft in computed peak water surface elevations or about 1 percent of the maximum flow depths, (2) 13 percent deviation in the computed peak discharges, (3) 0.5 percent change in the total attenuation of peak discharge incurred in the reach from the Teton Dam to the Shelly gaging station, and (4) 13 percent change in the flood-peak travel time at Shelly. These results indicate that Manning n has little effect on peak elevations or depths; however, the travel time is affected by more than one-half of the percentage change in the Manning n values.

A typical simulation of the Teton flood as described above involved 73 Δx reaches, 55 hrs of prototype time, and an initial time step (Δt) of 0.07 hrs which automatically increased gradually to 0.58 hrs. The simulation required only 30 seconds on the latest PC micro-computer.

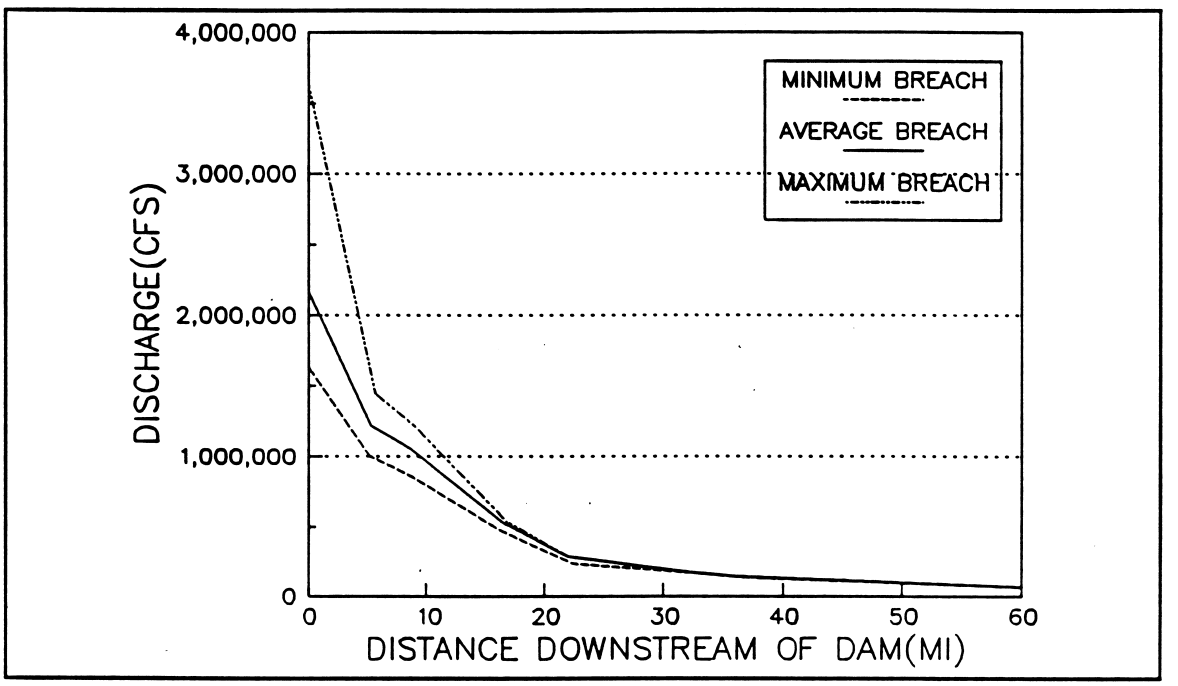

Figure 5.8 Profile of peak discharge from Teton Dam failure showing sensitivity of various breach parameters

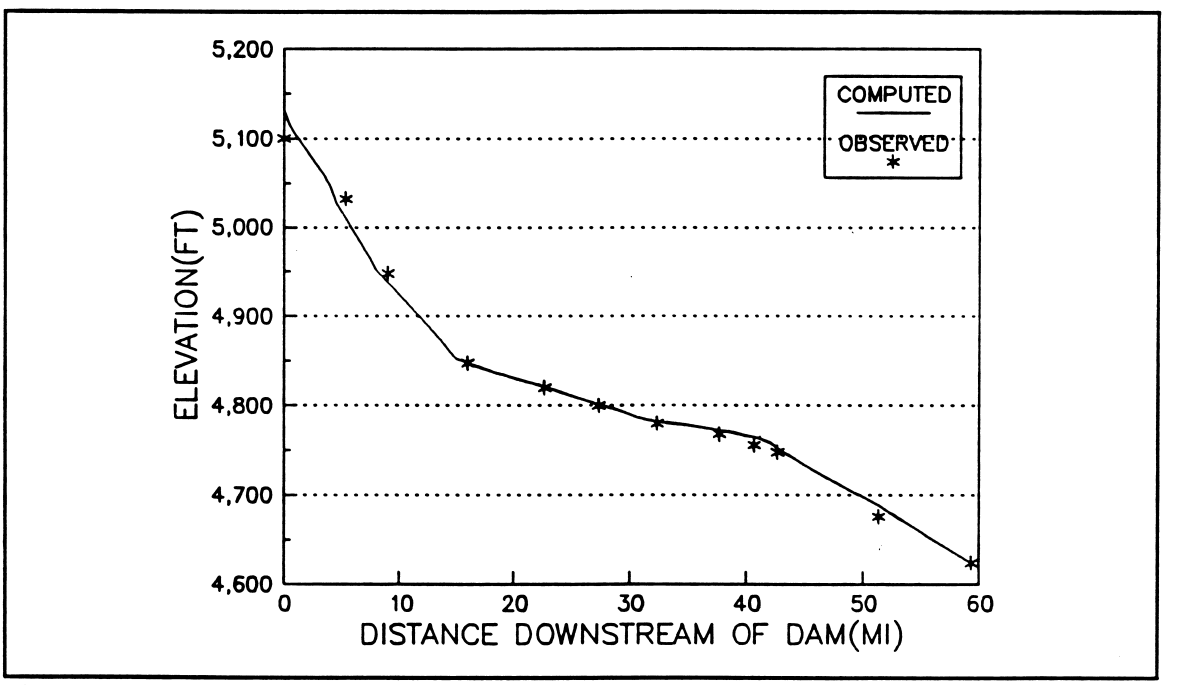

Figure 5.9 Profile of peak flood elevation from Teton Dam failure

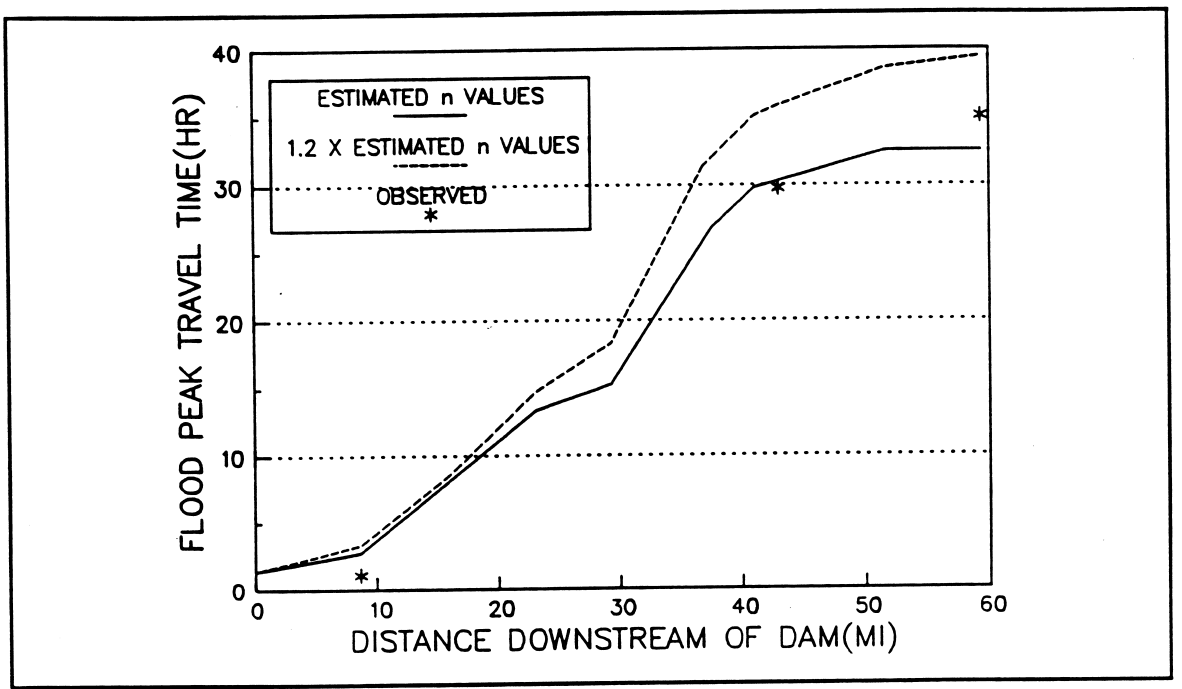

Figure 5.10 Travel time of flood peak from Teton Dam failure

5.6. UNCERTAINTIES OF DAM-BREACH FLOOD MODELING

Dam-breach flood modeling is subject to uncertainties due to the governing equations and the lack of exact specification of some of the model's parameters.

5.6.1 Two-Dimensional Effects

When the governing equations for routing hydrographs (unsteady flows) are the one-dimensional Saint-Venant equations, there are some instances where the flow is more nearly two-dimensional than one-dimensional, i.e., the velocity of flow and water surface elevations vary not only in the x-direction along the river/valley but also in the transverse direction perpendicular to the x-direction. Neglecting the two-dimensional nature of the flow can be important when the flow first expands onto an extremely wide and flat floodplain after having passed through an upstream reach which severely constricts the flow. In many cases where the wide floodplain is bounded by rising topography, the significance of neglecting the transverse velocities and water surface variations is confined to a transition reach in which the flow changes from one-dimensional to two-dimensional and back to one-dimensional along the x-direction. In this case, the use of radially defined cross sections along with judicious off-channel storage widths can minimize the two-dimensional effect neglected within the transition reach. The radial cross sections appear in plan-view as concentric circles of increasing diameter in the downstream direction which is considered appropriate for radial flow expanding onto a flat plane. The cross sections become perpendicular to the x-direction for the reach downstream of the transition reach. Where the very wide, flat floodplain appears unbounded, the radial representation of the cross sections is at best only an approximation which varies from reality the farther from the constricted section and the greater the variability of the floodplain topography and friction.

5.6.2 Cross-Sectional Degradation

The high velocity flows associated with dam-break floods can cause significant scour (degradation) of alluvial channels. This enlargement in channel cross-sectional area is neglected since the equations for sediment transport, sediment continuity, dynamic bed-form friction, and channel bed armoring are not included among the governing equations. The significance of the neglected alluvial channel degradation is directly proportional to the channel/floodplain conveyance ratio, since the characteristics of most floodplains along with their much lower flow velocities cause much less degradation within the floodplain. As this ratio increases, the degradation could cause a significant lowering of the water surface elevations until the flows are well within the recession limb of the dam-break hydrograph; however, in many instances this ratio is fairly small and remains such until the dam-break flood peak has attenuated significantly at locations far downstream of the dam, and where this occurs the maximum flow velocities also have attenuated. However, narrow channels with minimal floodplains are subject to overestimation of water elevations due to significant channel degradation. The alluvial fill (aggradation) occurring in the floodplain or in the channel during receding flows are considered to have relatively small effects on the flood conditions.

5.6.3 Manning n

The uncertainty associated with the selection of the Manning n can be quite significant for dam-break floods due to: (1) the great magnitude of the flood produces flow in portions of floodplains which were never before inundated; this necessitates the selection of the n value without the benefit of previous evaluations of n from measured elevation/discharges or the use of calibration techniques for determining the n values; (2) the effects of transported debris can alter the Manning n. Although the uncertainty of the Manning n may be large, this effect is considerably damped or reduced during the computation of the water surface elevations. Based on the Manning equation, the relationship between the error or uncertainty in the Manning n and the resulting flow depth is as follows:

$$d_e/d = (n_e/n)^{b'} \tag{5.69}$$

where:

$$b' = 3/(3m+5) \tag{5.70}$$

in which d_e is the flow depth associated with an erroneous n_e value, d is the flow depth associated with the correct n value, and m is a cross section shape factor, i.e., m = 0 for rectangular sections, m = 0.5 for parabolic, m = 1 for triangular, and $1 < m < 3$ for channels with floodplains (the wider and more flat the floodplain, the greater the m value). Since for channels with wide floodplains ($m \simeq 2$), the exponent b′ as defined by Eq. (5.70) is equal to 0.27; and from an inspection of Eq. (5.69) it is evident that the difference between d_e and d is substantially damped relative to the difference between n_e and n. In fact, if $n_e/n = 1.5$, then $d_e/d = 1.12$, which illustrates the degree of damping. Thus for rivers with wide floodplains the uncertainty in the Manning n results in considerably less uncertainty in the flow depths.

The propagation speed (c) of the floodwave is related to the uncertainty in the Manning n according to the following:

$$c_e/c = (n_e/n)^{0.67\,b'-1} \tag{5.71}$$

in which c_e is the propagation speed associated with an erroneous n_e value. If $n_e/n = 1.5$, then $c_e/c = 0.72$, which indicates less damping than that associated with Eq. (5.69). Thus errors in the Manning n affect the rate of propagation more than the flow depth, but in each instance the error is not proportional to the n_e error, but rather the error is damped.

When the range of probable Manning n values is fairly large, a sensitivity test should be made using a dam-breach flood routing model to simulate the flow, first with the lower estimated n values and then with the higher estimated n values. The resulting high water profiles computed along the river/valley for each simulation represent an envelope of possible flood peak elevations within the range of uncertainty associated with the estimated n values.

5.6.4 Debris Effects

Dam-break floods create a large amount of transported debris; this may accumulate at constricted cross sections such as bridge openings where it acts as a temporary dam and partially or completely restricts the flow. The maximum magnitude of this effect, i.e., the upper envelope of the flood peak elevation profile, can be approximated by using a dam-breach flood routing model to simulate the blocked constriction as a downstream dam having an estimated elevation-discharge relation approximating the gradual flow stoppage. Also, the downstream dam can be used to simulate the later rapid increase due to the release of the ponded waters when the debris dam is allowed to breach.

5.6.5 Breach Properties

The uncertainty associated with the breach parameters, especially $\bar{b}$ and τ, also cause uncertainty in the flood peak elevation profile and arrival times. The best approach is to perform a sensitivity test using minimum, average, and maximum values for $\bar{b}$ and τ. The maximum flood is produced by selecting the maximum probable $\bar{b}$ and minimum probable τ, whereas the minimum flood is produced by using the minimum probable $\bar{b}$ and maximum probable τ values. The differences in flood peak properties (flow, elevation, time of arrival) at any section downstream of the dam due to variations in the breach parameters reduces in magnitude or is damped as the dam-break flood propagates through the downstream river/valley.

5.6.6 Flow Losses

There is uncertainty associated with volume losses incurred by the flood as it propagates downstream and inundates large floodplains where infiltration and detention storage losses may occur. Such losses are difficult to predict. The conservative approach is to neglect such losses, unless very good reasons justify their consideration, e.g., observed losses associated with several previous large floods in the same floodplain.

REFERENCES

Arcement, G.J., Jr. and Schneider, V.R. (1984). Guide for Selecting Manning's Roughness Coefficients for Natural Channels and Flood Plains, Report No. RHWA-TS-84-204, U.S. Geological Survey for Federal Highway Administration, National Tech. Information Service, PB84-242585, 61 pp.

ASCE/USCOLD (1975). Lessons from Dam Incidents, USA, American Society of Civil Engineers, New York.

Barnes, H.H., Jr. (1967). Roughness Characteristics of Natural Channels, Geological Survey Water-Supply Paper 1849, U.S. Government Printing Office, Washington, DC, 213 pp.

Bechteler, W. and Broich, K. (1993). 'Computational Analysis of the Dam-Erosion Problem,' Advances in Hydro-Science and Engineering, Vol. 1, Wang, S.S.Y. (editor), Ctr. for Computational Hydroscience and Engineering, Univ. of Mississippi, pp. 723-728.

Chen, C.L. and Armbruster, J.T. (1980). 'Dam-Break Wave Model: Formulation and Verification,' J. Hydraul. Div., ASCE, Vol. 106, No. HY5, May, pp. 746-767.

Chow, V.T. (1959). Open-Channel Hydraulics, McGraw-Hill, New York.

Chow, V.T., Maidment, D.R., and Mays, L.W. (1988). Applied Hydrology, McGraw-Hill, New York.

Cristofano, E.A. (1965). Method of Computing Rate for Failure of Earth Fill Dams, Bureau of Reclamation, Denver, CO, April.

Cunge, J.A., Holly, F.M., Jr., and Verway, A. (1980). Practical Aspects of Computational River Hydraulics, Pitman, Boston, MA.

Davies, W.E., Bailey, J.F., and Kelly, D.B. (1972). 'West Virginia's Buffalo Creek Flood: A Study of the Hydrology and Engineering Geology,' Geological Survey Circular 667, U.S. Geological Survey, 32 pp.

DeLong, L.L. (1989). 'Mass conservation: 1-D Open Channel Flow Equations,' J. Hydraul. Div., Vol. 115, No. HY2, pp. 263-268.

Dressler, R.F. (1954). 'Comparison of Theories and Experiments for the Hydraulic Dam-Break Wave,' Internat. Assoc. Sci. Pubs., 3, No. 38, pp. 319-328.

Federal Investigative Board (1977). Report of Failure of Kelly Barnes Dam, Toccoa, Georgia, U.S. Army Corps of Engineers, Atlanta, GA.

Fread, D.L. (1971). 'Discussion of Implicit Flood Routing in Natural Channels,' by M. Amein and C. S. Fang, J. Hydraul. Div., ASCE, Vol. 97, No. HY7, pp. 1156-1159.

Fread, D.L. (1973). 'Technique for Implicit Dynamic Routing in Rivers with Tributaries,' Water Resources Research, Vol. 9, No. 4, pp. 918-926.

Fread, D.L. (1974). Numerical Properties of Implicit Four-Point Finite Difference Equations of Unsteady Flow, HRL-45, NOAA Tech. Memo NWS HYDRO-18, Hydrologic Research Laboratory, National Weather Service, Silver Spring, MD.

Fread, D.L. (1977). 'The Development and Testing of a Dam-Break Flood Forecasting Model,' Proc. of Dam-Break Flood Modeling Workshop, U.S. Water Resources Council, Washington, DC, pp. 164-197.

Fread, D.L. (1981). 'Some Limitations of Contemporary Dam-Break Flood Routing Models,' Preprint 81-525: Annual Meeting of American Society of Civil Engineers, Oct. 17, 1982, St. Louis, MO, Oct. 27, 15 pp.

Fread, D.L. (1983). 'Computational Extensions to Implicit Routing Models,' Proceedings of the Conference on Frontiers in Hydraulic Engineering, ASCE, MIT, Cambridge, MA, pp. 343-348.

Fread, D.L. (1984). 'A Breach Erosion Model for Earthen Dams,' Proceedings of Specialty Conference on Delineation of Landslides, Flash Flood, and Debris Flow Hazards in Utah, Utah State Univ., Logan, UT, June 15, 30 pp.

Fread, D.L. (1985). 'Channel Routing,' Hydrological Forecasting, (Eds: M.G. Anderson and T.P. Burt), John Wiley and Sons, New York, Chapter 14, pp. 437-503.

Fread, D.L. (1987). BREACH: An Erosion Model for Earthen Dam Failures, Hydrologic Research Laboratory, NOAA, NWS, U.S. Dept. of Commerce, Silver Spring, MD, June, 34 pp.

Fread, D.L. (1988). The NWS DAMBRK Model: Theoretical Background/User Documentation, HRL-256, Hydrologic Research Laboratory, National Weather Service, Silver Spring, MD, 315 pp.

Fread, D.L. (1989a). 'Flood Routing and the Manning n,' Proc. of the International Conference for Centennial of Manning's Formula and Kuichling's Rational Formula, (Ed: B.C. Yen), Charlottesville, VA, pp. 699-708.

Fread, D.L. (1989b). 'National Weather Service Models to Forecast Dam-Breach Floods,' Hydrology of Disasters (Eds: O. Starosolszky and O.M. Melder), Proc. of the World Meteorological Organization Tech. Conf., Nov. 1988, Geneva, Switzerland, pp. 192-211.

Fread, D.L. (1992). 'Flow Routing,' Handbook of Hydrology (Ed. D. Maidment), McGraw-Hill, New York, Chapter 10, pp. 10.1-10.36.

Fread, D.L. (1993). 'Selection of Δx and Δt Computational Steps for Four-Point Implicit Non-linear Dynamic Routing Models,' Proceedings, National Hydraulic Engineering Conference, ASCE, San Francisco.

Fread, D.L. and Harbaugh, T.E. (1971). 'Open Channel Profiles by Newton's Iteration Technique,' J. Hydrol., Vol. 13, pp. 70-80.

Fread, D.L. and Lewis, J.M. (1988). 'FLDWAV: A Generalized Flood Routing Model,' Proc. of National Conf. on Hydraulic Engr., ASCE, Colorado Springs, CO, pp. 668-673.

Fread, D.L., Jin, M., and Lewis, J.M., (1996). 'An LPI Numerical Implicit Solution for Unsteady Mixed-Flow Simulation,' Proceedings, North American Water and Environment Congress '96, ASCE, Anaheim, California.

Froehlich, D.C. (1987). 'Embankment-Dam Breach Parameters,' Proc. of the 1987 National Conf. on Hydraulic Engr., ASCE, New York, August, pp. 570-575.

Froehlich, D.C. (1995). 'Embankment Dam Breach Parameters Revisited,' First International Conference on Water Resources Engineering, Vol. 1, ASCE, San Antonio, Texas, pp. 887-891.

Hagen, V.K. (1982). 'Re-evaluation of Design Floods and Dam Safety,' Paper Presented at Fourteenth ICOLD Congress, Rio de Janeiro.

Harris, G.W. and Wagner, D.A. (1967). Outflow from Breached Dams, Univ. of Utah.

Henderson, F.M. (1966). Open Channel Flow, Macmillan Co., New York, pp. 285-287.

Hydrologic Engineering Center (1982). HEC-2 Water Surface Profiles Users Manual, U.S. Army Corps of Engineers, Davis, CA.

ICOLD (1973). Lessons from Dam Incidents, Abridged Edition, USCOLD, Boston, MA.

Jarrett, R.D. (1984). 'Hydraulics of High-Gradient Streams,' J. Hydraul. Div., ASCE, Vol. 110, No. HY11, Nov., pp. 1519-1539.

Jarrett, R.D. and Costa, J.E. (1982). Hydrology, Geomorphology, and Dam-Break Modeling of the July 15, 1982, Lawn Lake Dam and Cascade Lake Dam Failures, Larimer County, Co., U.S. Geological Survey, Open File Report 84-62, 109 pp.

Johnson, F.A. and Illes, P. (1976). 'A Classification of Dam Failures,' Water Power and Dam Construction, Dec., pp. 43-45.

Land, L.F. (1980). 'Evaluation of Selected Dam-Break Flood-Wave Models by Using Field Data,' U.S. Geological Survey, Water Resources Investigations 80-44, NSTL Station, MS, 54 pp.

Liggett, J.A. and Cunge, J.A. (1975). 'Numerical Methods of Solution of the Unsteady Flow Equations,' Unsteady Flow in Open Channels, Vol. I, (Eds: K. Mahmood and V. Yevjevich), Vol. I, Chapt. 4, Water Resource Pub., Fort Collins, CO, pp. 89-182.

Macchione, F. and Sirangelo, B. (1988). 'Study of Earth Dam Erosion due to Overtopping,' Hydrology of Disasters, Proc. of Tech. Conf. in Geneva, November 1988, Starosolszky, O. and Melder, O.M. (editors), James and James, London, pp. 212-219.

MacDonald, T.C. and Langridge-Monopolis, J. (1984). 'Breaching Characteristics of Dam Failures,' J. Hydraul. Div., ASCE, Vol. 110, No. HY5, May, pp. 567-586.

Middlebrooks, T.A. (1952). 'Earth-Dam Practice in the United States,' Centennial Transactions, ASCE, Paper No. 2620, pp. 697-722.

O'Brien, J.S. and Julien, P. (1984). 'Physical Properties and Mechanics of Hyper-concentrated Sediment Flows,' Delineation of Landslide, Flash Flood, and Debris Flow Hazards in Utah, Utah State Univ., Utah Water Research Laboratory, Logan, UT, (Ed: D.S. Bowles), General Series UWRL/G-85/03, pp. 260-279.

Ponce, V.M. and Tsivoglou, A.J. (1981). 'Modeling of Gradual Dam-Breaches,' J. Hydraul Div., ASCE, Vol. 107, No. HY6, pp. 829-838.

Preissmann, A. (1961). 'Propagation of Translatory Waves in Channels and Rivers,' in Proc., First Congress of French Assoc. for Computation, Grenoble, France, pp. 433-442.

Rajar, R. (1978). 'Mathematical Simulation of Dam-Break Flow,' J. Hydraul. Div., ASCE, Vol. 104, No. HY7, pp. 1011-1026.

Ray, H.A., Kjelstrom, L.C., Crosthwaite, E.G., and Low, W.H. (1976). 'The Flood in Southeastern Idaho from the Teton Dam Failure of June 5, 1976,' Unpublished open file report, U.S. Geological Survey, Boise, ID.

Ré, R. (1946). 'A Study of Sudden Water Release from a Body of Water to Canal by the Graphical Method,' La Houille Blanche (France), No. 3, pp. 181-187.

Ritter, A. (1892). 'The Propagation of Water Waves,' Ver. Deutsch Ingenieure Zeitschr. (Berlin), 36, Pt. 2, No. 33, pp. 947-954.

Sakkas, J.G. and Strelkoff, T. (1973). 'Dam-Break Flood in a Prismatic Dry Channel,' J. Hydraul. Div., ASCE, Vol. 99, No. HY12, Dec. pp. 2195-2216.

Saint-Venant, Barré de (1871). 'Theory of Unsteady Water Flow, with Application to River Floods and to Propagation of Tides in River Channels,' Computes rendus, Vol. 73, Acad. Sci., Paris, France, pp. 148-154, 237-240. (Translated into English by U.S. Corps of Engrs., No. 49-g, Waterways Experiment Station, Vicksburg, MS, 1949.)

Samuels, P.G. (1985). Models of Open Channel Flow Using Preissmann's Scheme, Cambridge Univ., Cambridge, England, pp. 91-102.

Schocklitsch, A. (1917). 'On Waves Created by Dam Breaches,' Adak. Wiss. (Vienna) Proc., 126, Pt. 2A, pp. 1489-1514.

Singh, K.P. and Snorrason A. (1982). 'Sensitivity of Outflow Peaks and Flood Stages to the Selection of Dam Breach Parameters and Simulation Models,' University of Illinois State Water Survey Division, Surface Water Section, Champaign, IL, June, 179 pp.

Singh, V.P. and Quiroga, C.A. (1988). 'Dimensionless Analytical Solutions for Dam Breach Erosion,' J. of Hydraul. Res., Vol. 26, No. 2, pp. 179-197.

Singh, V.P., Scarlatos, P.D., Collins, J.G. and Jourdan, M.R. (1988). 'Breach Erosion of Earthfill Dams (BEED) Model,' Natural Hazards, Vol. 1, pp. 161-180.

Smart, G.M. (1984). 'Sediment Transport Formula for Steep Channels,' J. Hydraul. Div., ASCE, Vol. 110, No. HY3, pp. 267-276.

Stoker, J.M. (1957). Water Waves, Interscience, New York, pp. 452-455.

Strelkoff, T. (1969). 'The One-dimensional Equations of Open-Channel Flow,' J. Hydraul. Div., ASCE, Vol. 95, No. HY3, pp. 861-874.

Su, S.T. and Barnes, A.H. (1970). 'Geometric and Frictional Effects on Sudden Releases,' J. Hydraul. Div., ASCE, Vol. 96, No. HY11, Nov., pp. 2185-2200.

U.S. Army Corps of Engineers (1961). 'Floods Resulting from Suddenly Breached Dams -- Conditions of High Resistance, Hydraulic Model Investigation,' Misc. Paper 2-374, Report 2, WES, Nov., 121 pp.

U.S. Army Corps of Engineers (1975). National Program of Inspection of Dams, Bul. I-4, Dept. of the Army, Office of Chief of Engineers, Washington, DC.

Wetmore, J.N. and Fread, D.L. (1984). 'The NWS Simplified Dam Break Flood Forecasting Model for Desk-Top and Hand-Held Microcomputers,' Printed and Distributed by the Federal Emergency Management Agency (FEMA), 1984, 122 pp.

Wurbs, R.A. (1986). Comparative Evaluation of Dam-Breach Flood Wave Models, Texas A&M Univ., College Station, TX, May, pp. 13-20.